A step-by-step procedure for pH model construction in aquatic systems

A. F. Hofmann, F. J. R. Meysman, K. Soetaert, J. J. Middelburg

Biogeosciences, 5, 227–251, 2008
www.biogeosciences.net/5/227/2008/

Biogeosciences

A step-by-step procedure for pH model construction in aquatic systems

A. F. Hofmann, F. J. R. Meysman, K. Soetaert, and J. J. Middelburg

Netherlands Institute of Ecology (NIOO-KNAW), Centre for Estuarine and Marine Ecology, P.O. Box 140, 4400 AC Yerseke, The Netherlands

Received: 27 September 2007 – Published in Biogeosciences Discuss.: 12 October 2007
Revised: 20 December 2007 – Accepted: 29 January 2008 – Published: 21 February 2008

Abstract. We present, by means of a simple example, a comprehensive step-by-step procedure to consistently derive a pH model of aquatic systems. As pH modelling is inherently complex, we make every step of the model generation process explicit, thus ensuring conceptual, mathematical, and chemical correctness. Summed quantities, such as total inorganic carbon and total alkalinity, and the influences of modeled processes on them are consistently derived. The different time scales of processes involved in the pH problem (biological and physical reactions: days; aquatic chemical reactions: fractions of seconds) give rise to a stiff equation system. Subsequent reformulations of the system reduce its stiffness, accepting higher non-linear algebraic complexity. The model is reformulated until numerically and computationally simple dynamical solutions, like a variation of the operator splitting approach (OSA) and the direct substitution approach (DSA), are obtained. As several solution methods are pointed out, connections between previous pH modelling approaches are established. The final reformulation of the system according to the DSA allows for quantification of the influences of kinetic processes on the rate of change of proton concentration in models containing multiple biogeochemical processes. These influences are calculated including the effect of re-equilibration of the system due to a set of acid-base reactions in local equilibrium. This possibility of quantifying influences of modeled processes on the pH makes the end-product of the described model generation procedure a powerful tool for understanding the internal pH dynamics of aquatic systems.

1 Introduction

Human activities have increased atmospheric CO_2 levels by 36% since pre-industrial times, and further increases are expected over the next decades (Prentice et al., 2001; Alley et al., 2007). Rising atmospheric CO_2 levels lead to an input of CO_2 into the oceans and to subsequent acidification of surface waters (e.g. Orr et al., 2005).

Against this background, it is of high importance to analyze the impact of different biogeochemical processes onto alkalinity and the pH of natural waters (Sarmiento and Gruber, 2006; Stumm and Morgan, 1996). In recent years, various pH modeling approaches have been developed. These range from simple empirical correlations (Bjerknes and Tjomsland, 2001), over neural network approaches (Moatar et al., 1999), to mechanistic biogeochemical models that include reactive transport descriptions of varying complexity (e.g. Luff et al., 2001; Jourabchi et al., 2005). Mechanistic models have the advantage that they not only reproduce pH but also allow the prediction of future changes, and enable quantitative analysis of the processes that govern pH. As a result, they are a powerful tool to understand the pH dynamics of aquatic systems.

However, there are still two pending problems with mechanistic pH models. The first issue relates to the apparent diversity of approaches. Most modeling approaches have been presented without cross linking to other methods. As a result, it is difficult to assess whether approaches are mutually consistent, i.e., whether they would predict the same pH dynamics for exactly the same underlying biogeochemical model. Moreover, it is not clear what the respective advantages of the different solution techniques are, and whether they yield the same amount of information with respect to pH dynamics. Only some approaches are able to quantify the individual contribution of modelled processes on the pH.

Correspondence to: A. F. Hofmann
(a.hofmann@nioo.knaw.nl)

Published by Copernicus Publications on behalf of the European Geosciences Union.

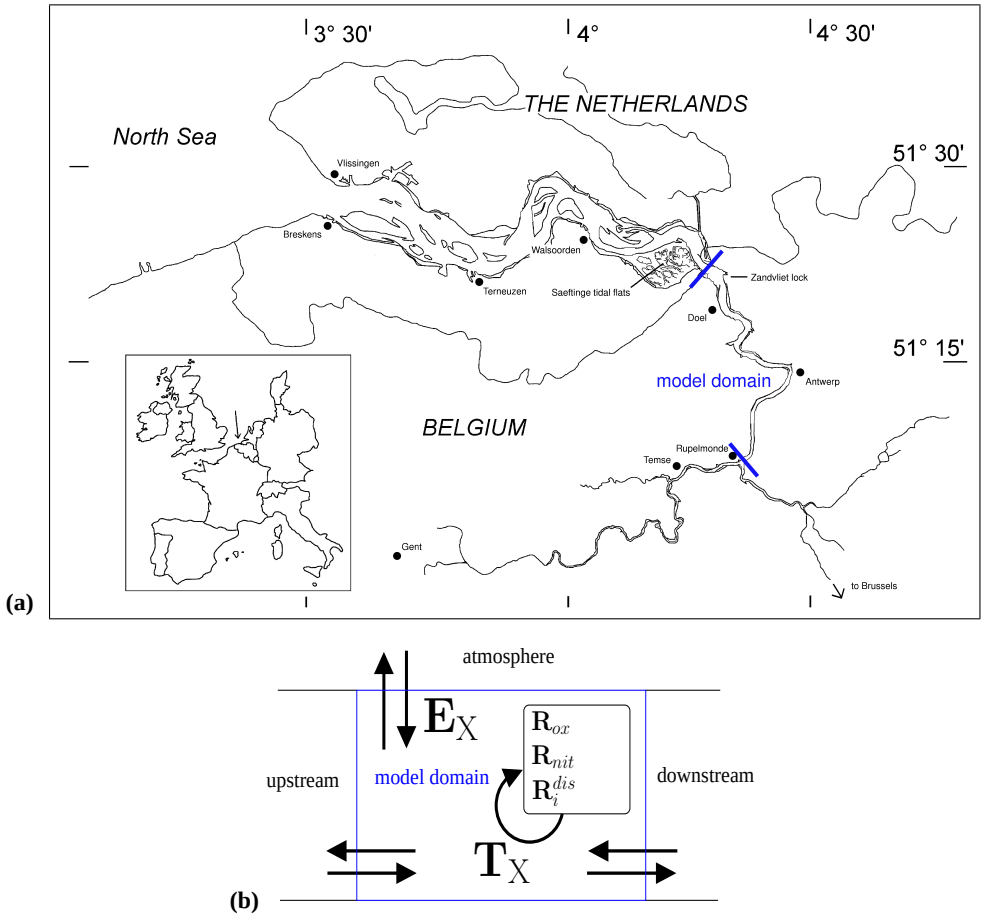

Fig. 1. (a): the example estuarine system: the model domain (the stretch of river between the blue lines) encompasses around 40 river kilometres; **(b)**: The model domain is represented by a conceptual model scheme with biogeochemical processes; For explanations of symbols, see text.

The second issue relates to the complexity of the present approaches. The construction of pH models is inherently complex, involving many sequential steps and assumptions. Furthermore, the different time scales of processes involved in the pH problem (biological and physical reactions: days; aquatic chemical reactions: fractions of seconds) give rise to a stiff equation system. It is important to deal with this complexity by making every assumption explicit and justifying every step. Even for a relatively simple biogeochemical system, the model generation procedure becomes quite lengthy and intricate. A disadvantage of recent pH modeling approaches is that they have been typically applied to complex reaction sets, generating lengthy expressions. The illustration of a complex solution procedure with a complex model is not always optimal. Accordingly, there is a clear need to illustrate the various approaches to model pH with a simple biogeochemical application.

The objective of the present study is to provide a generic step-by-step procedure to construct and solve a pH model for an aquatic system. We will illustrate this step-by-step approach using an example, i.e., by constructing an example pH model for a simple estuarine system. This example is simple enough to facilitate understanding, yet complex enough to illustrate all features of the pH modeling approach. Accordingly, the focus lies on concepts and principles rather than on mimicking the biogeochemical complexity of real aquatic systems. Models of more realistic and complex systems can be built by suitably changing the transport formulation or extending the reaction set. The feature of our analysis is that we carry out a number of sequential reformulations of the pH problem until elegant and efficient numerical solutions are possible. Along the way, we outline the implicit and explicit assumptions that are needed in every step of the procedure. This enables us to identify the weaknesses and strengths of past modeling procedures and solution methods. Our work therefore does not introduce a novel approach to pH modelling, but gives a systematic framework which encompasses existing approaches.

2 pH model construction: a step-by-step procedure

2.1 Step 1: Formulation of the model questions

Our example system is the upper Schelde estuary in northern Belgium (Fig. 1a). The model domain includes 40 km of river ranging from the inflow of the Rupel tributary to the Belgian-Dutch border. A set of characteristic parameters is given in the Results section. Our principal goal is to examine the pH changes associated with some (drastic) perturbations in the biogeochemistry of this estuary. Two types of changes to the system are examined:

1) The estuary receives municipal water from the city of Brussels, which is one of the last major European cities to implement a coordinated waste water treatment policy. In 2007, a new sewage treatment plant for 1.1 million inhabitants has started operating, and it is estimated that this will reduce the organic matter input to the estuary by 50%. How will the pH of the estuary react to this abrupt change? Which biogeochemical processes govern the pH steady state before and after the reduction?

2) Alongside the estuary lies the port of Antwerp, which concentrates one of the largest chemical industries in the world. The port harbours a large fertilizer industry with associated ship traffic of resources and products. Potential hazard scenarios include ship accidents with tankers carrying ammonia or ammonium-nitrate. What are the effects of such pulse-inputs on the estuarine pH and the influences of processes on it? Ammonia input and ammonium-nitrate input are examined as two separate perturbation scenarios.

2.2 Step 2: Formulation of the conceptual model

In general, the concentration of a chemical species [X] in an aquatic system is influenced by a set of physical (transport) processes $\mathbf{P}^j$, and a set of biogeochemical reactions $\mathbf{R}^i$. The resulting mass conservation equation (MCE) (Morel and Hering, 1993) reads

$$\frac{d[\mathrm{X}]}{dt} = \sum_j \mathbf{P}^j_{\mathrm{X}} + \sum_i \nu^i_{\mathrm{X}} \mathbf{R}^i \qquad (1)$$

where ν^i_{X} is the stoichiometric coefficient of species X in the i-th reaction. Throughout this paper, all species concentrations [X] are expressed as per kg of *solution* (gravimetric units per mass of solution). A crucial step in the model development is the decision which physical and biogeochemical processes to include in the model. This decision should be based on prior knowledge about the physics and biogeochemistry of the system. For our problem, two physical processes are of major relevance: advective-dispersive transport $\mathbf{T}_{\mathrm{X}}$ along the length axis of the river, and the exchange of volatile compounds with the atmosphere $\mathbf{E}_{\mathrm{X}}$. Although it would be possible here, no benthic exchange is taken into account to keep the mathematical expressions tractable. For the same reason, the estuary is modelled as a single box (Fig. 1b). Note that the implementation of a spatially explicit description would be entirely analogous in terms of pH modeling: the $\mathbf{T}_{\mathrm{X}}$ terms would simply give rise to partial rather than ordinary differential equations.

Table 1. Estimated rates (μmol-N $(\mathrm{kg}\cdot\mathrm{d})^{-1}$) of biogeochemical processes in the example system ((a): Soetaert and Herman, 1995a; (b): Andersson et al., 2006; (c): Soetaert and Herman, 1995b; (d): Middelburg et al., 1996).

pelagic primary production	$\mathbf{R}_{\mathrm{pri}}$	$\approx$	0.1	(a)
pelagic nitrification	$\mathbf{R}_{\mathrm{nit}}$	$\approx$	7.5	(b)
pelagic denitrification	$\mathbf{R}_{\mathrm{den}}$	$\approx$	6.1	(c)
pelagic oxic respiration	$\mathbf{R}_{\mathrm{ox}}$	$\approx$	2.9	(c)
benthic denitrification	$\mathbf{R}_{\mathrm{bden}}$	$\approx$	0.7	(c)
benthic oxic respiration	$\mathbf{R}_{\mathrm{box}}$	$\approx$	0.3	(d)

To assist in the selection of the biogeochemical reactions, Table 1 provides an overview of the relative importance of the various processes in the Schelde estuary. From the six biogeochemical reactions listed, we only retain pelagic oxic respiration $\mathbf{R}_{\mathrm{ox}}$ and pelagic nitrification $\mathbf{R}_{\mathrm{nit}}$. These are described according to reaction stoichiometries:

$$(\mathrm{CH_2O})_\gamma(\mathrm{NH_3}) + \gamma\ \mathrm{O_2} \rightarrow \mathrm{NH_3} + \gamma\ \mathrm{CO_2} + \gamma\ \mathrm{H_2O} \qquad (2a)$$

$$\mathrm{NH_4^+} + 2\mathrm{O_2} \rightarrow \mathrm{NO_3^-} + \mathrm{H_2O} + 2\mathrm{H^+} \qquad (2b)$$

With γ being the C/N ratio of organic matter (see Table 14).

Pelagic primary production, benthic denitrification and benthic respiration can be justifiably neglected compared to pelagic nitrification and pelagic oxic mineralization (Table 1). Pelagic denitrification was important in the 1970's, but, due to improved water quality, is now of minor significance (Soetaert et al., 2006). For this reason and for didactical purposes, we did not include it in the model (to avoid lengthy expressions in the mathematical derivations). However, we will include it a posteriori to check on the importance of denitrification in pH regulation of the model domain.

Since our aim is to model the pH, a number of acid-base reactions have to be accounted for. To select these reactions, we first have to constrain the set of chemical species that are modelled. For simplicity, we consider the estuary as an aqueous solution of the three most abundant seawater ions $\mathrm{Cl^-}$, $\mathrm{Na^+}$, and $\mathrm{SO_4^{2-}}$ (DOE, 1994). For a realistic model application other quantities like borate might be important, but we neglect these to keep the model as simple as possible. Furthermore, we also incorporate organic matter, nitrate, oxygen and the ammonium and carbonate systems, as these species feature in the retained reactions ($\mathbf{R}_{\mathrm{ox}}$ and $\mathbf{R}_{\mathrm{nit}}$, Eq. 2). Table 2 lists the set of acid-base dissociation reactions $\mathbf{R}^{\mathrm{dis}}_i$ that

Table 2. Acid-base reactions in the example system, thermodynamical pK_{HA}'s are infinite dilution values at 25°C as given in Stumm and Morgan (1996). According to the exclusion criterion given in Appendix A, reactions with an ϵ below 0.5 % are neglected. ϵ has been calculated for a desired pH range of 6 to 9, with $pK^*_{HA} \approx pK_{HA}$, and with [TA]=5000 μ mol kg^{-1} (estimated from upstream and downstream boundary conditions given in Table 14), and with total concentrations for the given system as listed (total nitrate and ammonium are measured values for the example model system, total carbon dioxide has been estimated and all other total quantities have been calculated from salinity S=5 according to DOE, 1994).

reaction ($HA \rightleftharpoons H^+ + A^-$)		**pK_{HA}**	$\frac{\sum A}{\mu mol\ kg^{-1}}$	$\frac{\epsilon}{\%}$
(1) HCl	$\rightleftharpoons H^+ + Cl^-$	−3	$2.8\ 10^4$	$5.6\ 10^{-7}$
(2) $Na^+ + H_2O$	$\rightleftharpoons H^+ + NaOH$	14	$2.4\ 10^4$	$4.8\ 10^{-3}$
(3) H_2SO_4	$\rightleftharpoons H^+ + HSO_4^-$	−3	$1.5\ 10^3$	$2.9\ 10^{-8}$
(4) HSO_4^-	$\rightleftharpoons H^+ + SO_4^{2-}$	2	$1.5\ 10^3$	$2.9\ 10^{-3}$
(5) HNO_3	$\rightleftharpoons H^+ + NO_3^-$	−1	$3.2\ 10^2$	$6.4\ 10^{-7}$
(6) NH_4^+	$\rightleftharpoons H^+ + NH_3$	9	$2.9\ 10^1$	*0.58*
(7) $CO_2 + H_2O$	$\rightleftharpoons H^+ + HCO_3^-$	6	$6.0\ 10^3$	*120*
(8) HCO_3^-	$\rightleftharpoons H^+ + CO_3^{2-}$	10	$6.0\ 10^3$	*12*
(9) H_2O	$\rightleftharpoons H^+ + OH^-$	16	$5.5\ 10^7$	0.11

involve all the mentioned chemical species. This finalizes the conceptual model formulation – see scheme in Fig. 1b.

2.3 Step 3: Constraining the model pH range – selection of acid-base reactions

Currently there are different definitions for pH in use, which all express the "protonating capability" of a solution. The difference between these so-called pH scales relates to the calibration buffers that are used in pH measurements, which then determine the type of equilibrium constants (K^* values) that should be used in calculations. A detailed description of these pH scales can be found, for example, in Dickson (1984) or Zeebe and Wolf-Gladrow (2001). Here, we model the free gravimetric proton concentration $[H^+]=[H_3O^+]$, and the associated pH scale is the *free hydrogen ion concentration scale* (Dickson, 1984), which is defined as

$$pH = -\log_{10}\left(\frac{[H^+]}{[H^+]_{ref}}\right) \tag{3b}$$

The reference proton concentration $[H^+]_{ref}$=1 mol kg^{-1} makes the argument of the logarithm dimensionless.

After the selection of the pH scale, we can proceed to a formal delineation of the pH range of the model. This setting of the pH range determines which dissociation reactions should be incorporated. Note that most pH modeling approaches do not explicitly mention this step. In these, the set of acid-base reactions is simply imposed without further consideration. However, models are simplified representations of reality, and they should be kept as simple as possible. This is particularly true for pH models, which are computationally demanding. Accordingly, one should avoid incorporating dissociation reactions that have no chance of affecting the pH dynamics.

Therefore, we propose a formal procedure for the selection of acid-base reactions which is based on prior knowledge about the buffering capacity and the possible pH range of the specific system. In our case, we know that the part of the Schelde estuary which we model is strongly buffered, as are most estuarine and marine systems, with a total alkalinity [TA] of $\approx$5000 μmol kg^{-1} (estimated from upstrean and downstream boundary conditions given in Table 14). We furthermore know that the pH only fluctuates over a range from 7.5 to 8. Nonetheless, we anticipate stronger excursions because of the quite drastic perturbation scenarios outlined above. Allowing a suitable margin, we require that the model should represent the pH dynamics properly within a pH range of 6 to 9. This constraint enables us to reduce the reaction set in Table 2 considerably.

Whether or not a certain acid-base system has to be taken into account depends on a combination of

1) its pK value(s) which tell us whether the speciation of the acid-base species will change within the pH range under consideration,

2) the total concentration of the acid [$\sum$ A] which tells us how large theoretical changes in [H^+] due to the speciation of the respective acid-base system would be in a completely unbuffered system, and

3) the mean [TA] of the system which tells us if these theoretical changes in [H^+] will be appreciable or negligible in a buffered aquatic system.

Appendix A details a formal selection procedure which integrates these three criteria into a single quantity ϵ for each acid-base system. ϵ represents the amount of protons ignored (theoretical unbuffered proton concentration offset) by neglecting the reaction in question, in percent of the average [TA] of the modeled system.

Finally, we exclude all reactions whose ϵ value is smaller than 0.5%. This means the total amount of protons which could be taken up or released in the model, if the reaction in question would be included and the pH reaches the border of the pH range, is less than half a percent of typical alkalinity levels of the system.

Note that polyprotic acids are treated as a set of monoprotic acids considering each dissociation step independently.

Applying this rule (ϵ values are given in Table 2), we do not need to incorporate the dissociation reactions of HCl, NaOH, H_2SO_4, HSO_4^-, HNO_3 and H_2O. Table 3 shows the reduced set of acid-base reactions considered in the model. Technically, it would not be "wrong" to include the other reactions. However, there is no reason to do so, provided that

Table 3. pH range adjusted set of acid-base reactions.

$\mathbf{R}^{\mathrm{dis}}_{\mathrm{NH_4^+}}$	$\mathrm{NH_4^+}$	$\rightleftharpoons$	$\mathrm{H^+ + NH_3}$
$\mathbf{R}^{\mathrm{dis}}_{\mathrm{CO_2}}$	$\mathrm{CO_2 + H_2O}$	$\rightleftharpoons$	$\mathrm{H^+ + HCO_3^-}$
$\mathbf{R}^{\mathrm{dis}}_{\mathrm{HCO_3^-}}$	$\mathrm{HCO_3^-}$	$\rightleftharpoons$	$\mathrm{H^+ + CO_3^{2-}}$

the simulated pH stays within the range [6–9] (this should be checked a posteriori).

Note that the auto-dissociation reaction of water is not included in Table 3. Effectively, this reaction has been treated in a rather arbitrary fashion in past models. The auto-dissociation of water is included in some models (e.g. Jourabchi et al., 2005), while excluded from others (e.g. Luff et al., 2001). Usually, the reasons for inclusion or exclusion are not mentioned. Here however, our formal selection procedure predicts that it is unimportant (we will check this a posteriori).

2.4 Step 4: A mass conservation equation (MCE) for each species

Overall, our model set includes a set of n_p=7 processes encompassing 5 reactions ($\mathbf{R}_{\mathrm{ox}}$, $\mathbf{R}_{\mathrm{nit}}$, $\mathbf{R}^{\mathrm{dis}}_{\mathrm{NH_4^+}}$, $\mathbf{R}^{\mathrm{dis}}_{\mathrm{CO_2}}$, $\mathbf{R}^{\mathrm{dis}}_{\mathrm{HCO_3^-}}$) and 2 transport processes ($\mathbf{T}_{\mathrm{X}}$, $\mathbf{E}_{\mathrm{X}}$) that feature a set of n_s=9 chemical species:

$$\mathrm{OM,\ O_2,\ NO_3^-,\ CO_2,\ HCO_3^-,\ CO_3^{2-},\ NH_4^+,\ NH_3,\ and\ H^+}$$

Note that organic matter $(\mathrm{CH_2O})_\gamma(\mathrm{NH_3})$ has been abbreviated by OM and that the concentrations of $\mathrm{Cl^-}$, $\mathrm{Na^+}$, $\mathrm{HSO_4^-}$, $\mathrm{SO_4^{2-}}$, NaOH and $\mathrm{OH^-}$ are not simulated, since they are not affected by the modeled processes[1].

Although $\mathrm{H_2O}$ does feature in the biogeochemical reactions retained in the model ($\mathbf{R}_{\mathrm{ox}}$ and $\mathbf{R}_{\mathrm{nit}}$; Eqs. (2a) and (2b)) and in the set of acid-base reactions (Table 3), its concentration is nevertheless considered constant (Morel and Hering, 1993). The resulting mass conservation equations for all 9 chemical species are given in Table 4, where again $\mathbf{T}_{\mathrm{X}}$ denotes advective-dispersive transport of chemical species X and $\mathbf{E}_{\mathrm{X}}$ denotes the exchange of chemical species X with the atmosphere.

At this point, a first attempt to solve the system can be made.

Solution method [1a]: Together with suitable initial conditions, the equation set in Table 4 represents an initial-value problem of ordinary differential equations (ODEs) (Fabian et al., 2001). Using suitable kinetic expressions for all modeled process rates (i.e. for the forward and backward rates for acid-base reactions), this system is fully determined. In principle, it can be directly solved by common numerical integration techniques, such as Euler or Runge-Kutta integration (Press et al., 1992) or more complex integration schemes. This solution procedure is referred to as the *Full Kinetic Approach (FKA)* (Steefel and MacQuarrie, 1996; Meysman, 2001).

[1] All species are of course affected by advective-dispersive transport $\mathbf{T}_{\mathrm{X}}$. It would be correct to include the transport of conservative ions (conservative with respect to all other processes except transport) in the model by a variable salinity which is advective-dispersively transported. However, we consider a constant salinity for the sake of didactical simplicity.

Table 4. Mass conservation equations (MCEs) for each chemical species.

(1)	$\frac{d[\mathrm{OM}]}{dt}$	=	$\mathbf{T}_{\mathrm{OM}} - \mathbf{R}_{\mathrm{ox}}$
(2)	$\frac{d[\mathrm{O_2}]}{dt}$	=	$\mathbf{T}_{\mathrm{O_2}} + \mathbf{E}_{\mathrm{O_2}}$-$\gamma\ \mathbf{R}_{\mathrm{ox}} - 2\ \mathbf{R}_{\mathrm{nit}}$
(3)	$\frac{d[\mathrm{NO_3^-}]}{dt}$	=	$\mathbf{T}_{\mathrm{NO_3^-}} + \mathbf{R}_{\mathrm{nit}}$
(4)	$\frac{d[\mathrm{CO_2}]}{dt}$	=	$\mathbf{T}_{\mathrm{CO_2}} + \mathbf{E}_{\mathrm{CO_2}} + \gamma\ \mathbf{R}_{\mathrm{ox}} - \mathbf{R}^{\mathrm{dis}}_{\mathrm{CO_2}}$
(5)	$\frac{d[\mathrm{HCO_3^-}]}{dt}$	=	$\mathbf{T}_{\mathrm{HCO_3^-}} + \mathbf{R}^{\mathrm{dis}}_{\mathrm{CO_2}} - \mathbf{R}^{\mathrm{dis}}_{\mathrm{HCO_3^-}}$
(6)	$\frac{d[\mathrm{CO_3^{2-}}]}{dt}$	=	$\mathbf{T}_{\mathrm{CO_3^{2-}}} + \mathbf{R}^{\mathrm{dis}}_{\mathrm{HCO_3^-}}$
(7)	$\frac{d[\mathrm{NH_4^+}]}{dt}$	=	$\mathbf{T}_{\mathrm{NH_4^+}}$ - $\mathbf{R}^{\mathrm{dis}}_{\mathrm{NH_4^+}} - \mathbf{R}_{\mathrm{nit}}$
(8)	$\frac{d[\mathrm{NH_3}]}{dt}$	=	$\mathbf{T}_{\mathrm{NH_3}} + \mathbf{E}_{\mathrm{NH_3}} + \mathbf{R}_{\mathrm{ox}} + \mathbf{R}^{\mathrm{dis}}_{\mathrm{NH_4^+}}$
(9)	$\frac{d[\mathrm{H^+}]}{dt}$	=	$\mathbf{T}_{\mathrm{H^+}} + 2\ \mathbf{R}_{\mathrm{nit}} + \mathbf{R}^{\mathrm{dis}}_{\mathrm{CO_2}} + \mathbf{R}^{\mathrm{dis}}_{\mathrm{HCO_3^-}} + \mathbf{R}^{\mathrm{dis}}_{\mathrm{NH_4^+}}$

For the reaction $\mathbf{R}^{\mathrm{dis}}_{\mathrm{NH_4^+}}$, for example, suitable kinetic expressions for the forward and backward reaction would be

$$\left(\mathbf{R}^{\mathrm{dis}}_{\mathrm{NH_4^+}}\right)_{\mathrm{forward}} = k_f\ [\mathrm{NH_4^+}] \tag{4b}$$

$$\left(\mathbf{R}^{\mathrm{dis}}_{\mathrm{NH_4^+}}\right)_{\mathrm{backward}} = k_b\ [\mathrm{NH_3}][\mathrm{H^+}] \tag{5b}$$

with $\mathbf{R}^{\mathrm{dis}}_{\mathrm{NH_4^+}} = \left(\mathbf{R}^{\mathrm{dis}}_{\mathrm{NH_4^+}}\right)_{\mathrm{forward}} - \left(\mathbf{R}^{\mathrm{dis}}_{\mathrm{NH_4^+}}\right)_{\mathrm{backward}}$ and k_f and k_b being the forward and backward rate constants. Zeebe and Wolf-Gladrow (2001) give formulations for forward and backward rate constants of some acid-base systems relevant in seawater. However, problems arise when the values of the rate constants are not available.

Solution method [1b]: One way to avoid this problem is to adopt the principle of microscopic reversibility or detailed balancing (Morel and Hering, 1993), which requires the quotient of the kinetic forward and backward rate constants k_f and k_b to be equal to the equilibrium constant of the reaction ($\frac{k_f}{k_b} = K^*$).

Table 5. Characteristic time τ of processes to be modeled. Values for $\mathbf{R}^{\mathrm{dis}}_{\mathrm{NH_4^+}}$ and $\mathbf{R}^{\mathrm{dis}}_{\mathrm{CO_2}}$ are obtained from Zeebe and Wolf-Gladrow (2001), and $\mathbf{R}^{\mathrm{dis}}_{\mathrm{HCO_3^-}}$ from Morel and Hering (1993). Values for the remaining processes are estimated from Tables 1 and 14. For the exchange with the atmosphere, piston velocities K_L as given by Raymond and Cole (2001) were used.

(1)	$\mathbf{R}_{\mathrm{ox}}$	10	*d*
(2)	$\mathbf{R}_{\mathrm{nit}}$	4	*d*
(3)	$\mathbf{T}_{\mathrm{X}}$	13	*d*
(4)	$\mathbf{E}_{\mathrm{X}}$	4	*d*
(5)	$\mathbf{R}^{\mathrm{dis}}_{\mathrm{NH_4^+}}$	10	*s*
(6)	$\mathbf{R}^{\mathrm{dis}}_{\mathrm{CO_2}}$	10^{-7}	*s*
(7)	$\mathbf{R}^{\mathrm{dis}}_{\mathrm{HCO_3^-}}$	10^{-2}	*s*

Based on this principle, e.g., $\mathbf{R}^{\mathrm{dis}}_{\mathrm{NH_4^+}}$ can be written as

$$\mathbf{R}^{\mathrm{dis}}_{\mathrm{NH_4^+}} = k_f \left([\mathrm{NH_4^+}] - \frac{[\mathrm{NH_3}][\mathrm{H^+}]}{K^*_{\mathrm{NH_4^+}}} \right) \tag{6b}$$

which only features the forward rate constant k_f. Assuming a sufficiently high value for k_f this is an approximation of the local equilibrium assumption (Steefel and MacQuarrie, 1996) which will be discussed later.

Although it overcomes the problem of undetermined kinetic rate constants, solution method 1b does not resolve a serious limitation of the FKA: it is bound to lead to very long computation times and numerical problems. The reason for this problem is that the transport and reaction processes that are included in the model occur on widely different time scales. Table 5 gives approximative values for the characteristic time scale τ for each process.

These characteristic time scales span several orders of magnitude, ranging from microseconds to days. This phenomenon is called numerical *stiffness* (Boudreau, 1996b). Problems that are numerically stiff basically require special integration methods or rather small time steps in order to ensure accuracy. Effectively, the process with the smallest characteristic time scale will set the pace of how the integration procedure progresses with time. Given the small time scales of the acid base reactions, pH models are very impractical or virtually impossible to solve with the FKA, even with integration methods that are specifically geared towards stiff problems (Chilakapati et al., 1998). A runtime comparison of all our presented approaches, including the FKA (solution method 1b), is given at the end of the paper.

In conclusion, the FKA does not form a good choice for pH problems. As shown below, more refined alternatives to the FKA exist which do not depend on well constrained acid-base forward and backward rate constants[2] and which drastically reduce the computation time by reducing the stiffness of the system.

Table 6. Kinetic and equilibrium processes and species. n_x denotes the number of respective species or processes.

species	kinetic	OM, O_2, NO_3^-	n_{ks} = 3
(n_s=9)	equilibrium	CO_2, HCO_3^-, CO_3^{2-}, NH_4^+, NH_3, H^+	n_{es} = 6
processes	kinetic	$\mathbf{R}_{\mathrm{ox}}$, $\mathbf{R}_{\mathrm{nit}}$, $\mathbf{T}_{\mathrm{X}}$, $\mathbf{E}_{\mathrm{X}}$	n_{kp} = 4
(n_p=7)	equilibrium	$\mathbf{R}^{\mathrm{dis}}_{\mathrm{NH_4^+}}$, $\mathbf{R}^{\mathrm{dis}}_{\mathrm{CO_2}}$, $\mathbf{R}^{\mathrm{dis}}_{\mathrm{HCO_3^-}}$	n_{ep} = 3

2.5 Step 5: Kinetic and equilibrium processes and species

Table 5 shows that the characteristic time scales cluster in two groups. There is a group of comparatively slow processes happening on a timescale of days (Processes 1 to 4) and a group of comparatively fast processes happening on timescales of fractions of a second to seconds (Processes 5 to 7). If the rate of one process is "sufficiently fast" compared to that of another process, this process can be assumed in local equilibrium on the timescale of the "slower" process (e.g. Olander, 1960; Aris and Mah, 1963; Otto and Quinn, 1971; DiToro, 1976; Saaltink et al., 1998). This allows to group the processes into slow *kinetic processes*, whose kinetics enter the model via suitable expressions, and fast *equilibrium processes*, whose kinetics are neglected, i.e., local equilibrium is assumed to be reached instantaneously at any time.

The designation of processes as "kinetic" or "equilibrium" also entails a corresponding classification of the species. *Kinetic species* are those species whose concentrations are exclusively influenced by kinetic processes, while *equilibrium species* are species that take part in at least one equilibrium reaction.

The grouping in kinetic and equilibrium processes depends on the minimal time resolution of the model simulations (cf. Saaltink et al., 1998) That means, the reference time to which to compare processes as "fast" and "slow" is the integration timestep of the model. In our model simulations, the goal is to examine the pH changes over a period of days to weeks, resulting in an integration timestep of about one minute.

Accordingly, we assume the kinetics of reactions whose characteristic time scales are less than one minute to be negligible. Table 6 provides the resulting grouping of processes and species.

Note that local equilibrium is an assumption that is commonly used for systems to which our pH modelling approach

[2] Still, rough estimates of the kinetic rate constants for all reactions are necessary to estimate the corresponding time scales for step 5.

Table 7. Kinetic process formulations. $[X]_{up}$ represents the upstream concentration of species X, $[X]_{down}$ its downstream concentration, and $[X]_{sat}$ its saturation concentration.

$\mathbf{R}_{ox}$	=	$r_{ox} \cdot [OM] \cdot \left([O_2]/\left([O_2] + ks_{O_2}\right)\right)$
$\mathbf{R}_{nit}$	=	$r_{nit} \cdot [NH_4{}^+] \cdot \left([O_2]/\left([O_2] + ks_{O_2}\right)\right)$
$\mathbf{T}_X$	=	$(Q/V) \cdot \left([X]_{up} - [X]\right)$
		$+(E'/V) \cdot ([X]_{up} + [X]_{down} - 2 \cdot [X])$
$\mathbf{E}_X$	=	$(K_L/d_w) \cdot ([X]_{sat} - [X])$

is geared: macroscopic aquatic systems that contain reactions on the timescale of several days as well as fast acid-base reactions. For models on this temporal and spatial scale, assuming local equilibrium does not change the model results.

However, the assignment of a process to the kinetic or equilibrium group is not absolute: it depends on the model time-scale, and hence, on the questions addressed by the model. In our case, the exchange with the atmosphere is catalogued as a kinetic process. However, in a model that describes the pH evolution in the ocean over a million year time-scale, exchange with the atmosphere can be considered an equilibrium process. Similarly, the dissociation Reactions (5) to (7) are classified as equilibrium processes in our model. Yet, in a model that focuses on the fast relaxation of intracellular pH (model time-scale of fractions of seconds), these same Reactions (5) to (7) would be considered kinetic reactions[3].

The Processes (1) to (4) from Table 5 are modeled kinetically, and hence, we need to provide suitable constitutive expressions for their process rates . We describe oxic respiration and nitrification as first order processes with respect to [OM] and $[NH_4^+]$ respectively, and with a Monod dependency on $[O_2]$. The advective-dispersive transport is simply modeled as an exchange across the upstream and downstream system boundaries. The exchange with the atmosphere is described by the classical reaeration mechanism (Thomann and Mueller, 1987). Table 7 lists the resulting kinetic expressions, parameters are given and explained in Table 14.

2.6 Step 6: Mathematical closure of the system – the mass action laws

Although the kinetics of the processes considered to be in local equilibrium are neglected, these reactions are still part of the model. If the concentrations of species on either side of the reaction equation changes, the equilibrium shifts according to Le Chatelier's principle. However, the rate of this shift is not governed by the kinetics of the equilibrium reaction themselves since they are assumed to be infinitely fast (local equilibrium is reached instantaneously). The net equilibrium

[3]However, then the rates of reactions on the time scale of our slow kinetic reactions can be assumed to be zero.

Table 8. Fully determined explicit DAE system. Note that the dissociation constants used are stoichiometric constants (denoted by the star as superscript; in contrast to thermodynamic constants; see Zeebe and Wolf-Gladrow (2001) for a description of different dissociation constants).

$\frac{d[OM]}{dt}$	=	$\mathbf{T}_{OM}$ - $\mathbf{R}^{dis}_{ox}$
$\frac{d[O_2]}{dt}$	=	$\mathbf{T}_{O_2} + \mathbf{E}_{O_2} - \gamma\, \mathbf{R}^{dis}_{ox} - 2\, \mathbf{R}^{dis}_{nit}$
$\frac{d[NO_3^-]}{dt}$	=	$\mathbf{T}_{NO_3^-} + \mathbf{R}^{dis}_{nit}$
$\frac{d[CO_2]}{dt}$	=	$\mathbf{T}_{CO_2} + \mathbf{E}_{CO_2} + \gamma\, \mathbf{R}^{dis}_{ox} - \mathbf{R}^{dis}_{CO_2}$
$\frac{d[HCO_3^-]}{dt}$	=	$\mathbf{T}_{HCO_3^-} + \mathbf{R}^{dis}_{CO_2} - \mathbf{R}^{dis}_{HCO_3^-}$
$\frac{d[CO_3^{2-}]}{dt}$	=	$\mathbf{T}_{CO_3^{2-}} + \mathbf{R}^{dis}_{HCO_3^-}$
$\frac{d[NH_4^+]}{dt}$	=	$\mathbf{T}_{NH_4^+} - \mathbf{R}^{dis}_{nit} - \mathbf{R}^{dis}_{NH_4^+}$
$\frac{d[NH_3]}{dt}$	=	$\mathbf{T}_{NH_3} + \mathbf{E}_{NH_3} + \mathbf{R}^{dis}_{ox} + \mathbf{R}^{dis}_{NH_4^+}$
$\frac{d[H^+]}{dt}$	=	$\mathbf{T}_{H^+} + 2\, \mathbf{R}^{dis}_{nit} + \mathbf{R}^{dis}_{CO_2} + \mathbf{R}^{dis}_{HCO_3^-} + \mathbf{R}^{dis}_{NH_4^+}$
0	=	$[H^+][HCO_3^-] - K^*_{CO_2}[CO_2]$
0	=	$[H^+][CO_3^{2-}] - K^*_{HCO_3^-}[HCO_3^-]$
0	=	$[H^+][NH_3] - K^*_{NH_4^+}[NH_4^+]$

reaction rates $\mathbf{R}^{dis}$ are non-zero quantities and only depend on the supply rates of reactants and products of the equilibrium reaction in question due to slow kinetic processes in the model. In solution method 1b we approximated the local equilibrium assumption by calculating, e.g., $\mathbf{R}^{dis}_{NH_4^+}$ by equation 6b using a very high value for k_f. However, under the true local equilibrium assumption the equilibrium is reached "instantaneously" which means

$$k_f \to \infty \tag{7a}$$

and

$$\left([NH_4^+] - \frac{[NH_3][H^+]}{K^*_{NH_4^+}}\right) \to 0 \tag{7b}$$

The latter expression is the equilibrium mass action law (Morel and Hering, 1993). This multiplication of an infinite quantity with 0 renders the net equilibrium reaction rates $\mathbf{R}^{dis}$ into mathematical unknowns. Chemical reasoning tells us that they are finite quantities.

As a result, the system in Table 4 becomes an underdetermined system with 9 equations (the MCE's) and 12 unknowns (9 species concentrations and the 3 equilibrium reaction rates). To solve this system, it has to be mathematically closed by adding the equilibrium mass-action laws of the equilibrium reactions as additional algebraic constraints.

Including the mass action laws results in a fully determined initial-value differential algebraic equation (DAE)

Table 9. Model transformed into the canonical form: a fully determined implicit initial-value DAE system. The combined mass conservation equations obtained by this transformation are equivalent to the result of a series of linear combinations of the MCEs from Table 4: (4)+(5)+(6); (7)+(8); and (5)+2·(6)+(8)−(9).

differential MCEs of kinetic species			
(1)	$\frac{d[\mathrm{OM}]}{dt}$	=	$\mathbf{T}_{\mathrm{OM}} - \mathbf{R}_{\mathrm{ox}}$
(2)	$\frac{d[\mathrm{O_2}]}{dt}$	=	$\mathbf{T}_{\mathrm{O_2}} + \mathbf{E}_{\mathrm{O_2}} - \gamma\,\mathbf{R}_{\mathrm{ox}} - 2\,\mathbf{R}_{\mathrm{nit}}$
(3)	$\frac{d[\mathrm{NO_3^-}]}{dt}$	=	$\mathbf{T}_{\mathrm{NO_3^-}} + \mathbf{R}_{\mathrm{nit}}$
combined differential MCEs of equilibrium species			
(4)	$\frac{d[\mathrm{CO_2}]}{dt} + \frac{d[\mathrm{HCO_3^-}]}{dt} + \frac{d[\mathrm{CO_3^{2-}}]}{dt}$	=	$\mathbf{T}_{\mathrm{CO_2}} + \mathbf{T}_{\mathrm{HCO_3^-}} + \mathbf{T}_{\mathrm{CO_3^{2-}}} + \mathbf{E}_{\mathrm{CO_2}} + \gamma\,\mathbf{R}_{\mathrm{ox}}$
(5)	$\frac{d[\mathrm{NH_3}]}{dt} + \frac{d[\mathrm{NH_4^+}]}{dt}$	=	$\mathbf{T}_{\mathrm{NH_3}} + \mathbf{T}_{\mathrm{NH_4^+}} + \mathbf{E}_{\mathrm{NH_3}} + \mathbf{R}_{\mathrm{ox}} - \mathbf{R}_{\mathrm{nit}}$
(6)	$\frac{d[\mathrm{HCO_3^-}]}{dt} + 2\frac{d[\mathrm{CO_3^{2-}}]}{dt} + \frac{d[\mathrm{NH_3}]}{dt} - \frac{d[\mathrm{H^+}]}{dt}$	=	$\mathbf{T}_{\mathrm{HCO_3^-}} + 2\,\mathbf{T}_{\mathrm{CO_3^{2-}}} + \mathbf{T}_{\mathrm{NH_3}} - \mathbf{T}_{\mathrm{H^+}} + \mathbf{E}_{\mathrm{NH_3}} + \mathbf{R}_{\mathrm{ox}} - 2\,\mathbf{R}_{\mathrm{nit}}$
algebraic constraints (AEs): mass-action laws			
(7)	0	=	$[\mathrm{H^+}][\mathrm{HCO_3^-}] - K^*_{\mathrm{CO_2}}[\mathrm{CO_2}]$
(8)	0	=	$[\mathrm{H^+}][\mathrm{CO_3^{2-}}] - K^*_{\mathrm{HCO_3^-}}[\mathrm{HCO_3^-}]$
(9)	0	=	$[\mathrm{H^+}][\mathrm{NH_3}] - K^*_{\mathrm{NH_4^+}}[\mathrm{NH_4^+}]$

system (Fabian et al., 2001) (Table 8). The structure of this DAE system can be generalized as:

$$\frac{dy}{dt} = f(t, y, z) \tag{8a}$$

$$0 = g(y) \tag{8b}$$

where t is time. The DAE system is split into two parts: a differential part containing differential equations (Eq. 8a), and an algebraic part containing equations with no differentials (Eq. 8b). It also contains two types of variables: the variables y whose differentials $\frac{dy}{dt}$ are present (*differential variables* – the species concentrations) and the variables z whose differentials are absent (*algebraic variables* – the unknown equilibrium reaction rates $\mathbf{R}_{\mathrm{NH_4^+}}$, $\mathbf{R}_{\mathrm{CO_2}}$, and $\mathbf{R}_{\mathrm{HCO_3^-}}$). The algebraic part of the DAE system (Eq. 8b) only contains the differential variables y, and not the algebraic variables z (the equilibrium reaction rates). As can be seen from Table 8, the DAE system is fully determined (12 equations for 12 unknowns).

To our knowledge, this DAE system cannot be numerically integrated in the above form, despite being fully determined. To this end, the DAE system has to be reformulated first. For example, the DASSL routine (Differential Algebraic System Solver; Petzold, 1982) can solve implicit DAE systems (with suitable initial conditions given) of the form:

$$F\left(t, y, \frac{dy}{dt}\right) = 0 \tag{9}$$

This means that, if one wants to use the DASSL solver, the DAE equations may contain differentials of more than one variable (i.e., implicit differential equations), but the whole equation system can no longer contain the algebraic variables z. In the next step, we will discuss a suitable transformation that brings the DAE system in Table 8 in a form that can be solved by DASSL.

2.7 Step 7: Reformulation 1: transformation into the canonical form

The system can be brought into a DASSL-solvable form by means of a *transformation into the canonical form* as discussed in, e.g., DiToro (1976), Steefel and MacQuarrie (1996), Lichtner (1996), Saaltink et al. (1998), Chilakapati et al. (1998) and Meysman (2001), based on an idea put forward by Aris and Mah (1963). During this transformation, the unknown equilibrium reaction rates are eliminated from the system. In a system with n_{es} equilibrium species and n_{ep} equilibrium reactions, the n_{es} differential MCEs of the equilibrium species are then replaced by $n_{ei}{=}n_{es}{-}n_{ep}$ combined MCEs which do no longer contain the unknown equilibrium reaction rates. Appendix B details this procedure for our problem. In our case the transformation of the system into the canonical form results in the reformulated DAE system as given in Table 9, which contains 9 variables and 9 equations. Note that the transformation procedure also provides explicit expressions for the unknown net equilibrium reaction terms $\mathbf{R}^{\mathrm{dis}}_{\mathrm{CO_2}}$, $\mathbf{R}^{\mathrm{dis}}_{\mathrm{HCO_3^-}}$, and $\mathbf{R}^{\mathrm{dis}}_{\mathrm{NH_4^+}}$ (see Appendix B). These can be used as output variables in the model and are sometimes of interest.

*Solution method [2]:*The model in Table 9 can be directly solved with the differential algebraic system solver DASSL (Petzold, 1982). This approach is referred to as the *Full Numerical Approach (FNA).*

Still, this full numerical approach is not the most elegant way to approach the pH calculation. The equation set is supplied "as it is" to an external numerical solver routine, which then performs the number crunching. A further reformulation explicitly takes advantage of the chemical structure of the pH problem, thus allowing for less demanding numerical methods.

2.8 Step 8: Introduction of equilibrium invariants

The Eqs. (4) to (6) of Table 9 contain differentials of more than one species on their left-hand sides. This means the differential part of the DAE system is not explicit and cannot be solved by common integration methods such as Euler integration. To obtain a single differential on the left-hand side, one can introduce composite variables – as done in Table 10 for our model. These composite concentration variables are referred to as *equilibrium invariants*. The reason for

Table 10. Composite variables to create explicit ODEs in Table 9.

A	:=	$[CO_2] + [HCO_3^-] + [CO_3^{2-}]$	$\triangleq$	$[\sum CO_2]$
B	:=	$[NH_3] + [NH_4^+]$	$\triangleq$	$[\sum NH_4^+]$
C	:=	$[HCO_3^-] + 2[CO_3^{2-}] + [NH_3] - [H^+]$	$\triangleq$	[TA]

this nomenclature is straightforward. The right hand sides of Eqs. (4) to (6) do no longer contain the equilibrium reaction rates, and as a consequence, the rate of change of the equilibrium invariants is not influenced by the equilibrium reactions. Chemically, these equilibrium invariants thus can be seen as quantities that are conservative or invariant with respect to the equilibrium reactions. Note that the definition of the equilibrium invariants introduces n_{ei}=3 new variables. To keep the DAE system determined, the definitions of the equilibrium invariants have to be added.

The equilibrium invariants are in fact familiar quantities. We immediately recognize A and B as the dissolved inorganic carbon (DIC) and total ammonium concentrations, which are denoted $[\sum CO_2]$ and $[\sum NH_4^+]$. The third equilibrium invariant is termed total alkalinity [TA]. Again it has a familiar form: it is a subset of the total alkalinity [TA] as defined by Dickson (1981). Still a number of subtleties should be stressed:

1) In our approach, the definition of total alkalinity follows naturally from the transformation into the canonical form and the elimination of the equilibrium process rates. It is not postulated a priori like in many previous pH modeling procedures (e.g. Regnier et al., 1997; Luff et al., 2001; Jourabchi et al., 2005).

2) The alkalinity definition is linked to a particular choice of kinetic and equilibrium reactions. Accordingly, when the reaction set is modified, the alkalinity definition might change as well. Also, even when keeping the same reaction set but choosing a different model timescale, one could arrive at a different alkalinity definition.

3) In our transformation procedure into canonical form we deliberately select suitable row operations during the Gauss-Jordan elimination (Appendix B) such that we obtain a subset of Dickson's total alkalinity as an equilibrium invariant. Sticking to this practice, modifications in the reaction set and in the model time-scale, as mentioned above, might result in different subsets of Dickson's total alkalinity. However, if this practice is abandoned, also different related quantities like, for example, the "sum of excess negative charge" as used by Soetaert et al. (2007) can be obtained.

4) The right-hand side of the [TA] equation (Eq. (6) in Table 9) does not contain the rate of any equilibrium reaction. This immediately shows that the alkalinity is a true equilibrium invariant, i.e., [TA] is not influenced by equilibrium reactions, even though all its constituents are affected by these reactions[4].

5) The influence of kinetic processes on [TA] can be directly inferred from the right-hand side of the [TA] equation (Eq. (6) in Table 9). This implies that one does not need to invoke the electroneutrality of the solution or the notion of "explicit conservative total alkalinity" as advocated by Wolf-Gladrow et al. (2007) to obtain the influences of kinetic processes on [TA].

Table 11. The model system written in tableau notation (Morel and Hering, 1993) with corresponding mole balance equations including their equivalence to our equilibrium invariants.

species	components		
	CO_2	NH_4^+	H^+
CO_2	1		
HCO_3^-	1		-1
CO_3^{2-}	1		-2
NH_4^+		1	
NH_3		1	-1
H^+			1

$TOTCO_2 = [CO_2] + [HCO_3^-] + [CO_3^{2-}] \triangleq [\sum CO_2]$
$TOTNH_4 = [NH_4^+] + [NH_3] \triangleq [\sum NH_4^+]$
$TOTH = -[HCO_3^-] - 2[CO_3^{2-}] - [NH_3^+] + [H^+] \triangleq -[TA]$

Note that the concept of equilibrium invariants is based on ideas put forward by amongst others DiToro (1976), Boudreau (1987), Boudreau and Canfield (1988), Boudreau (1991), Boudreau and Canfield (1993), and Morel and Hering (1993). Furthermore, as illustrated in Table 11, transforming the system into the canonical form and introducing equilibrium invariants is a formal mathematical way of finding suitable *components* in the *tableau* notation of Morel and Hering (1993) including the corresponding mole balance equations.

Note also that the sum of the transport terms on the right-hand side of the MCE's for the equilibrium invariants (Eqs. (4–6) in Table 9) can be directly calculated from the concentrations of the equilibrium invariants if the transport formulation for all species is the same, i.e., there is no differential transport in the model. Mathematically that means that the transport formulation needs to be distributive over the sum. In our model, for example, this is realized by assuming the same bulk dispersion coefficient E' for all chemical species.

[4]Similarly the temperature invariance of [TA] can be inferred, since on the timescale of an integration timestep, temperature only influences the acid-base equilibrium reactions (via the K^*'s), and these do not influence [TA].

Table 12. System refomulated in terms of equilibrium invariants: explicit ODEs and equilibrium species as functions of $[H^+]$ and equilibrium invariants.

MCEs of kinetic species		
(1)	$\frac{d[OM]}{dt}$	$= \mathbf{T}_{OM}$ - $\mathbf{R}_{ox}$
(2)	$\frac{d[O_2]}{dt}$	$= \mathbf{T}_{O_2} + \mathbf{E}_{O_2}$ - $\gamma\ \mathbf{R}_{ox}$ - 2 $\mathbf{R}_{nit}$
(3)	$\frac{d[NO_3^-]}{dt}$	$= \mathbf{T}_{NO_3^-} + \mathbf{R}_{nit}$
MCEs of equilibrium invariants		
(4)	$\frac{d[\sum CO_2]}{dt}$	$= \mathbf{T}_{CO_2} + \mathbf{T}_{HCO_3^-} + \mathbf{T}_{CO_3^{2-}} + \mathbf{E}_{CO_2} + \gamma\ \mathbf{R}_{ox}$
(5)	$\frac{d[\sum NH_4^+]}{dt}$	$= \mathbf{T}_{NH_3} + \mathbf{T}_{NH_4^+} + \mathbf{E}_{NH_3} + \mathbf{R}_{ox}$ - $\mathbf{R}_{nit}$
(6)	$\frac{d[TA]}{dt}$	$= \mathbf{T}_{HCO_3^-} + 2\ \mathbf{T}_{CO_3^{2-}} + \mathbf{T}_{NH_3}$ - $\mathbf{T}_{H^+} + \mathbf{E}_{NH_3} + \mathbf{R}_{ox}$ - 2 $\mathbf{R}_{nit}$
algebraic constraints (AEs)		
(7)	$[CO_2] = \frac{[H^+]^2}{[H^+]^2+K^*_{CO_2}[H^+]+K^*_{CO_2}K^*_{HCO_3^-}}[\sum CO_2]$	$\triangleq f_1^c\left([H^+]\right)\cdot[\sum CO_2]$
(8)	$[HCO_3^-] = \frac{K^*_{CO_2}[H^+]}{[H^+]^2+K^*_{CO_2}[H^+]+K^*_{CO_2}K^*_{HCO_3^-}}[\sum CO_2]$	$\triangleq f_2^c\left([H^+]\right)\cdot[\sum CO_2]$
(9)	$[CO_3^{2-}] = \frac{K^*_{CO_2}K^*_{HCO_3^-}}{[H^+]^2+K^*_{CO_2}[H^+]+K^*_{CO_2}K^*_{HCO_3^-}}[\sum CO_2]$	$\triangleq f_3^c\left([H^+]\right)\cdot[\sum CO_2]$
(10)	$[NH_4^+] = \frac{[H^+]}{[H^+]+K^*_{NH_4^+}}[\sum NH_4^+]$	$\triangleq f_1^n\left([H^+]\right)\cdot[\sum NH_4^+]$
(11)	$[NH_3] = \frac{K^*_{NH_4^+}}{[H^+]+K^*_{NH_4^+}}[\sum NH_4^+]$	$\triangleq f_2^n\left([H^+]\right)\cdot[\sum NH_4^+]$
(12)	$[TA] = [HCO_3^-] + 2\ [CO_3^{2-}] + [NH_3] - [H^+]$	

2.9 Step 9: Reformulation 2: Operator splitting

The algebraic part of our DAE system now consists of the mass action relations (Eqs. (7–9) in Table 9) and the definitions of the equilibrium invariants (Table 10). These equations feature the equilibrium species. However, each of the equilibrium species concentrations ($[CO_2]$, $[HCO_3^-]$, $[CO_3^{2-}]$, $[NH_3]$ and $[NH_4^+]$) can be readily expressed in terms of the proton concentration $[H^+]$ and the associated equilibrium invariants ($[\sum CO_2]$ and $[\sum NH_4^+]$). Appendix C describes this reformulation of the algebraic part of the DAE system. As a result, we obtain a novel DAE system (Table 12) where both the DE part and the AE part are reformulated in terms of the equilibrium invariants.

Solution method [3a]: Although it still can be directly solved with DASSL, the system given in Table 12 can be solved with less numerical effort using the *Operator Splitting Approach (OSA)*. This two step approach decouples the DAE system into an ordinary differential equation (ODE) system describing the kinetic reactions and an algebraic equation (AE) system that governs the equilibrium part (Luff et al., 2001; Meysman, 2001).

At each time step, the differential equation system is numerically integrated, e.g., with an Euler integration routine (Press et al., 1992), which provides values for the differential variables (kinetic species and equilibrium invariants) at the next time step. Subsequently, the algebraic equation system is solved at each timestep using the values for the differential variables provided by the numerical integration of the ODE system. Due to its nonlinearity in $[H^+]$, the algebraic equation system must be solved numerically (e.g. using the van Wijngaarden-Dekker-Brent or Newton-Raphson methods given by Press et al., 1992) to find the chemically meaningful root ($f([H^+])=0$) of the function:

$$\begin{aligned} f([H^+]) &= [TA] - \left([HCO_3^-] + 2\ [CO_3^{2-}] + [NH_3] - [H^+]\right) \\ &= [TA] - \left(\left(f_2^c\left([H^+]\right) + 2\cdot f_3^c\left([H^+]\right)\right)\cdot[\sum CO_2]\right. \\ &\quad \left. + f_1^n\left([H^+]\right)\cdot[\sum NH_4^+] - [H^+]\right) \end{aligned} \quad (10)$$

The classical OSA (solution method 3a) takes advantage of the specific structure of the model to solve it in a more elegant fashion than the FNA using DASSL. Still it requires at each time step the iteration between a numerical integration solver and a numerical root-finding technique, which might be computationally demanding.

Solution method [3b]: Recently, a modified OSA has been proposed (Follows et al., 2006), which is computationally faster. Rather than solving Eq. (10) directly, it acknowledges that carbonate alkalinity ([CA]=[HCO_3^-]+2[CO_3^{2-}]) contributes most to total alkalinity.

In our case, using the proton concentration of the previous timestep $[H^+]_{prev}$ and modelled equilibrium invariants (here [TA] and $[\sum NH_4^+]$), the modelled carbonate alkalinity can be estimated by:

$$[CA] \approx [TA] - f_1^n\left([H^+]_{prev}\right) \cdot [\sum NH_4^+] - [H^+]_{prev} \quad (11)$$

which allows a first guess for the $[H^+]$ at the current time step by analytically solving the quadratic equation:

$$\begin{aligned} 0 = {} & [CA][H^+]^2 + K^*_{CO_2}\left([CA] - [\sum CO_2]\right)[H^+] \\ & + K^*_{CO_2} K^*_{HCO_3^-}\left([CA] - 2[\sum CO_2]\right) \end{aligned} \quad (12)$$

This first guess for $[H^+]$ is then used to evaluate Eq. (10) and test if its root has been found (with sufficient accuracy). If not, the first guess for $[H^+]$ is used to calculate a better estimate for [CA] and the procedure is iteratively repeated. Iteration is mostly not necessary for buffered systems.

Note that this method also works if there are more minor contribution terms to [TA] than in our simple example. Note further that this method is inspired by the classical pH calculation methods of Culberson (1980), who analytically solved a cubic equation for systems with total alkalinity consisting of carbonate and borate alkalinity only, and Ben-Yaakov (1970), who iteratively solved an equation for $[H^+]$ by starting with an initial guess and by subsequent uniform increment of $[H^+]$.

Although this improved OSA approach (solution method 3b) is advantageous, it does not allow assessing the influences of modelled kinetic processes on the pH. A further reformulation of the system is possible, which avoids numerical root-finding as well as the iterative procedure according to Follows et al. (2006). This method allows for the assessment of the influences of modelled kinetic processes (including subsequent re-equilibration of the system) on the pH.

2.10 Step 10: Reformulation 3: Direct substitution

The classical OSA needs a numerical root-finding procedure because the algebraic equation (AE) part is non-linear with respect to the unknown proton concentration $[H^+]$. Therefore, if one could make $[H^+]$ a differential variable, its value would be known before the solution of the algebraic equation system. This way, the algebraic equation system could be solved analytically and the numerical root-finding procedure would not be necessary. To achieve this goal, the differential equation for [TA] in Table 12 should be substituted by a differential equation in $[H^+]$. Partially following the ideas developed by Jourabchi et al. (2005) and Soetaert et al. (2007), this can be done by starting with the total derivative of the equilibrium invariant [TA].

Equation (12) in Table 12 tells us, that if all the dissociation constants (K*'s) are constant, the equilibrium invariant [TA] can be written as a function of exclusively the proton concentration and the equilibrium invariants

$$[TA] = f\left([H^+], [\sum CO_2], [\sum NH_4^+]\right) \quad (13)$$

These variables are functions of time t. Consequently, the total derivative of [TA] can be written as

$$\begin{aligned} \frac{d[TA]}{dt} = {} & \frac{d[H^+]}{dt}\frac{\partial[TA]}{\partial[H^+]}\bigg|_{c,n} + \frac{d[\sum CO_2]}{dt}\frac{\partial[TA]}{\partial[\sum CO_2]}\bigg|_{h,n} \\ & + \frac{d[\sum NH_4^+]}{dt}\frac{\partial[TA]}{\partial[\sum NH_4^+]}\bigg|_{h,c} \end{aligned} \quad (14)$$

The subscripts indicate which quantities are held constant upon differentiation, and the shorthand notation c=[$\sum CO_2$], n=[$\sum NH_4^+$] and h=[H^+] has been used. Eq. (14) can be readily solved for $\frac{d[H^+]}{dt}$, resulting in

$$\begin{aligned} \frac{d[H^+]}{dt} = {} & \left(\frac{d[TA]}{dt} - \left(\frac{d[\sum CO_2]}{dt}\frac{\partial[TA]}{\partial[\sum CO_2]}\bigg|_{h,n}\right.\right. \\ & \left.\left. + \frac{d[\sum NH_4^+]}{dt}\frac{\partial[TA]}{\partial[\sum NH_4^+]}\bigg|_{h,c}\right)\right) \Bigg/ \frac{\partial[TA]}{\partial[H^+]}\bigg|_{c,n} \end{aligned} \quad (15)$$

Equation (15) can replace the differential equation for [TA] in Table 12. Each of the quantities on the right hand-side of Eq. (15) is explicitly known. The time derivatives of the equilibrium invariants are given by expressions (4)–(6) in Table 12. Furthermore, Appendix D1 shows how the partial derivatives of total alkalinity can be analytically calculated. Table 13 shows the reformulated DE's/MCE's of the DAE system. The AE part is the same as given in Table 12 (except for the equation for [TA] which is obsolete) and is not repeated.

The quantity $\frac{\partial[TA]}{\partial[H^+]}$ is a central and important quantity for pH modelling, as it modulates the effect of changes in state variables on $[H^+]$. Soetaert et al. (2007) call a similar quantity the *buffering capacity* of the solution, and Frankignoulle (1994) refers to the inverse of a related quantity as the *chemical buffer factor* of the solution.

*Solution method [4]:*The explicit ODE system in Table 13 can be numerically integrated. Subsequently, the AE system is used to analytically calculate the equilibrium concentrations for every timestep of the numerical integration. The resulting approach is referred to as the *Direct Substitution Approach (DSA)* (Saaltink et al., 1998; Meysman, 2001).

The DSA is the end result of three sequential reformulations of the pH problem. The DSA has two advantages. The first

Table 13. ODE part of the DAE system with direct substitution of $\frac{d[\mathrm{TA}]}{dt}$ by $\frac{d[\mathrm{H^+}]}{dt}$

kinetic species
$\frac{d[\mathrm{OM}]}{dt} = \mathbf{T}_{\mathrm{OM}}$ - $\mathbf{R}_{\mathrm{ox}}$
$\frac{d[\mathrm{O_2}]}{dt} = \mathbf{T}_{\mathrm{O_2}} + \mathbf{E}_{\mathrm{O_2}}$ - $\gamma\ \mathbf{R}_{\mathrm{ox}}$ - 2 $\mathbf{R}_{\mathrm{nit}}$
$\frac{d[\mathrm{NO_3^-}]}{dt} = \mathbf{T}_{\mathrm{NO_3^-}} + \mathbf{R}_{\mathrm{nit}}$
equilibrium invariants
$\frac{d[\sum \mathrm{CO_2}]}{dt} = \mathbf{T}_{\mathrm{CO_2}} + \mathbf{T}_{\mathrm{HCO_3^-}} + \mathbf{T}_{\mathrm{CO_3^{2-}}} + \mathbf{E}_{\mathrm{CO_2}} + \gamma\ \mathbf{R}_{\mathrm{ox}}$
$\frac{d[\sum \mathrm{NH_4^+}]}{dt} = \mathbf{T}_{\mathrm{NH_3}} + \mathbf{T}_{\mathrm{NH_4^+}} + \mathbf{E}_{\mathrm{NH_3}} + \mathbf{R}_{\mathrm{ox}}$ - $\mathbf{R}_{\mathrm{nit}}$
equilibrium species
$\frac{d[\mathrm{H^+}]}{dt} = \left(\mathbf{T}_{\mathrm{HCO_3^-}} + 2\,\mathbf{T}_{\mathrm{CO_3^{2-}}} + \mathbf{T}_{\mathrm{OH^-}} + \mathbf{T}_{\mathrm{NH_3}} - \mathbf{T}_{\mathrm{H^+}} + \mathbf{E}_{\mathrm{NH_3}} + \mathbf{R}_{\mathrm{ox}} - 2 \cdot \mathbf{R}_{\mathrm{nit}}\right) \Big/ \left.\frac{\partial[\mathrm{TA}]}{\partial[\mathrm{H^+}]}\right\vert_{c,n} - \left(\mathbf{T}_{\mathrm{CO_2}} + \mathbf{T}_{\mathrm{HCO_3^-}} + \mathbf{T}_{\mathrm{CO_3^{2-}}} + \mathbf{E}_{\mathrm{CO_2}} + \gamma \mathbf{R}_{\mathrm{ox}}\right) \left.\frac{\partial[\mathrm{TA}]}{\partial[\sum \mathrm{CO_2}]}\right\vert_{h,n} \Big/ \left.\frac{\partial[\mathrm{TA}]}{\partial[\mathrm{H^+}]}\right\vert_{c,n} - \left(\mathbf{T}_{\mathrm{NH_3}} + \mathbf{T}_{\mathrm{NH_4^+}} + \mathbf{E}_{\mathrm{NH_3}} + \mathbf{R}_{\mathrm{ox}} - \mathbf{R}_{\mathrm{nit}}\right) \left.\frac{\partial[\mathrm{TA}]}{\partial[\sum \mathrm{NH_4^+}]}\right\vert_{h,c} \Big/ \left.\frac{\partial[\mathrm{TA}]}{\partial[\mathrm{H^+}]}\right\vert_{c,n}$

advantage is that it makes maximal use of the chemical structure of the pH problem, to gain understanding and insight and to reduce the numerical effort. However, depending on the application, the OSA improved according to Follows et al. (2006) might have about the same computational requirements. The second and major advantage is that Eq. (15) directly quantifies the influence of the various kinetic processes on $[\mathrm{H^+}]$ and hence on pH. To show this, one can rearrange Eq. (15) (or rather the last equation in Table 13) to the form

$$\frac{d[\mathrm{H^+}]}{dt} = \alpha_{\mathbf{R}_{\mathrm{ox}}}\mathbf{R}_{\mathrm{ox}} + \alpha_{\mathbf{R}_{\mathrm{nit}}}\mathbf{R}_{\mathrm{nit}} + \alpha_{\mathbf{E}_{\mathrm{CO_2}}}\mathbf{E}_{\mathrm{CO_2}} + \alpha_{\mathbf{E}_{\mathrm{NH_3}}}\mathbf{E}_{\mathrm{NH_3}} + \sum \mathbf{T} \tag{16}$$

where the α coefficients and $\sum \mathbf{T}$ can be calculated at each time step using the expressions given in Appendix D2. The α-coefficients are modulating factors that express the influence on pH for each of the four kinetic reactions/processes. Similarly, the term $\sum \mathbf{T}$ lumps the influence of advective-dispersive transport processes on pH.

Splitting up α coefficients into process specific modulation factors and the buffering capacity of the solution, the influences of kinetic processes (except transport) on the rate of change of the proton concentration can be formalized as:

$$\alpha_{\mathbf{R}_X}\mathbf{R}_X = \left(\beta_{\mathbf{R}_X} \Big/ \frac{\partial[\mathrm{TA}]}{\partial[\mathrm{H^+}]}\right) \mathbf{R}_X \tag{17}$$

where the β coefficients represent the process specific modulation factors, which can also be found in Table D2 in Appendix D2.

The influence of transport on the rate of change of the proton concentration can be written as

$$\sum \mathbf{T} = \left(\mathbf{T}_{\mathrm{TA}} - \mathbf{T}_{\sum \mathrm{CO_2}} \left.\frac{\partial[\mathrm{TA}]}{\partial[\sum \mathrm{CO_2}]}\right\vert_{h,n} - \mathbf{T}_{\sum \mathrm{NH_4^+}} \left.\frac{\partial[\mathrm{TA}]}{\partial[\sum \mathrm{NH_4^+}]}\right\vert_{h,c}\right) \Big/ \frac{\partial[\mathrm{TA}]}{\partial[\mathrm{H^+}]} \tag{18}$$

with

$$\mathbf{T}_{\mathrm{TA}} = \mathbf{T}_{\mathrm{HCO_3^-}} + 2\,\mathbf{T}_{\mathrm{CO_3^{2-}}} + \mathbf{T}_{\mathrm{NH_3}} - \mathbf{T}_{\mathrm{H^+}} \tag{19}$$

$$\mathbf{T}_{\sum \mathrm{CO_2}} = \mathbf{T}_{\mathrm{CO_2}} + \mathbf{T}_{\mathrm{HCO_3^-}} + \mathbf{T}_{\mathrm{CO_3^{2-}}} \tag{20}$$

$$\mathbf{T}_{\sum \mathrm{NH_4^+}} = \mathbf{T}_{\mathrm{NH_3}} + \mathbf{T}_{\mathrm{NH_4^+}} \tag{21}$$

This means that the influence of a modelled kinetic process (except transport) on the $\frac{d[\mathrm{H^+}]}{dt}$ can be calculated by multiplying the kinetic rate of the process in question by a modulating factor β divided by the buffering capacity of the solution $\frac{\partial[\mathrm{TA}]}{\partial[\mathrm{H^+}]}$. The influence of transport on $\frac{d[\mathrm{H^+}]}{dt}$, however, is an expression of the transport terms for the equilibrium invariants divided by, again, the buffering capacity of the solution.

3 Results

3.1 Baseline simulation

In a first step, we performed a baseline steady state calculation for our model estuary with boundary conditions for the year 2004, which serves as a reference situation for the two perturbations scenarios outlined in the introduction. Table 14 provides an overview of the parameters and boundary conditions that were used in this baseline simulation.

Using the set of parameter values in Table 14, the DSA approach (solution method 4) was implemented within the modeling environment FEMME (Soetaert et al., 2002). The FORTRAN model code can be obtained from the author or downloaded from the FEMME website: http://www.nioo.knaw.nl/ceme/femme/.

The upstream concentrations were used as initial conditions, and a time-dependent simulation was performed until steady-state was reached. Table 15 compares the concentrations in the baseline simulation with values averaged over the year 2004. There is a good agreement between measured and modeled values. Also, the steady state rates for oxic mineralisation ($\mathbf{R}_{\mathrm{ox}}$=2.8 μmol-N kg^{-1} d^{-1}) and nitrification ($\mathbf{R}_{\mathrm{nit}}$=8.2 μmol-N kg^{-1} d^{-1}) are in good agreement with values from Table 1. This correspondence between model and measurements was obtained without tuning of model parameters. This provides confidence that the baseline simulation captures the essential features of the carbon and nitrogen

Table 14. *Characteristic parameters of the model domain*: K_L has been calculated by using a k_{600} value (piston velocity), normalized to a Schmidt number of 600 (the value for carbon dioxide in freshwater at 20°C), for the Schelde at Antwerp from Borges et al. (2004), and a Schmidt number for carbon dioxide at a temperature of 12 °C and a salinity of 5 from Wanninkhof (1992). r_{ox} has been obtained by dividing pelagic oxic mineralisation rates from Soetaert and Herman (1995b) by measured $[OM]$ values for 2004. r_{nit} has been calculated in similar fashion using nitrification rates obtained from Andersson et al. (2006). $[CO_2]_{sat}$ has been calculated according to a formula given in Weiss (1974) and atmospheric carbon dioxide levels from Borges et al. (2004). All dissociation constants are on the free hydrogen ion scale and for a temperature of T=12 °C and salinity S=5. *Boundary conditions of the model domain*: Values for $[\sum CO_2]$ have been obtained from Hellings et al. (2001). All other values are NIOO monitoring values for 2004, except for the values for [TA] which have been consistently calculated. "NM 2004" refers to measured data from 2004 obtained by the NIOO monitoring program.

Parameters					
Volume		V	108 798 000	m^3	(Soetaert and Herman, 1994)
Freshwater flow		Q	100	$m^3\,s^{-1}$	(Heip, 1988)
Bulk dispersion coefficient		E'	160	$m^3\,s^{-1}$	(Soetaert and Herman, 1994)
Mean water depth		d_w	10	m	(Soetaert and Herman, 1994)
Residence time		t_r	14	d	(Soetaert and Herman, 1994)
Piston velocity		K_L	2.8	$m\,d^{-1}$	(Borges et al., 2004; Wanninkhof, 1992)
First order oxic mineralisation rate		r_{ox}	0.1	d^{-1}	(Soetaert and Herman, 1995b), NM 2004
First order nitrification rate		r_{nit}	0.26	d^{-1}	(Andersson et al., 2006), NM 2004
Oxygen inhibition half saturation constant		ks_{O_2}	20.0	μmol-O_2 kg^{-1}	(Soetaert and Herman, 1995b)
Carbon to nitrogen ratio of organic matter		γ	8	mol-C mol-N^{-1}	(Soetaert and Herman, 1995b)
Mean water temperature		T	12	°C	NM 2004
Mean salinity		S	5		NM 2004
CO_2 saturation concentration		$[CO_2]_{sat}$	19	$\mu mol\,kg^{-1}$	(Weiss, 1974; Borges et al., 2004)
O_2 saturation concentration		$[O_2]_{sat}$	325	$\mu mol\,kg^{-1}$	(Garcia and Gordon, 1992)
NH_3 saturation concentration		$[NH_3]_{sat}$	0.0001	$\mu mol\,kg^{-1}$	estimated
Dissociation constant of CO_2		$K^*_{CO_2}$	$6.93\,10^{-1}$	$\mu mol\,kg^{-1}$	(Roy et al., 1993)
Dissociation constant of HCO_3^-		$K^*_{HCO_3^-}$	$2.59\,10^{-4}$	$\mu mol\,kg^{-1}$	(Roy et al., 1993)
Dissociation constant of NH_4^+		$K^*_{NH_4^+}$	$2.23\,10^{-4}$	$\mu mol\,kg^{-1}$	(Millero, 1995)
Ion product of H_2O		$K^*_{H_2O}$	$7.30\,10^{-3}$	$\left(\mu mol\,kg^{-1}\right)^2$	(Millero, 1995)
Boundary conditions					
			upstream	*downstream*	
organic matter concentration		[OM]	50	25	μmol-N kg^{-1}	NM 2004
nitrate		$[NO_3^-]$	350	260	$\mu mol\,kg^{-1}$	NM 2004
oxygen		$[O_2]$	70	240	$\mu mol\,kg^{-1}$	NM 2004
total ammonium		$[\sum NH_4^+]$	80	7	$\mu mol\,kg^{-1}$	NM 2004
total carbon dioxide		$[\sum CO_2]$	7100	4400	$\mu mol\,kg^{-1}$	(Hellings et al., 2001)
free protons		[H]	0.025	0.0121	$\mu mol\,kg^{-1}$	NM 2004
total alkalinity		[TA]	6926	4416	$\mu mol\,kg^{-1}$	calculated

dynamics, and thus provides a good starting point for the dynamic perturbation simulations.

Mass balance closure was verified for carbon, nitrogen and oxygen. The CO_2 export to the atmosphere ($\mathbf{E}_{CO_2}$=$-40.8\,\mu$mol-C $kg^{-1}\,d^{-1}$) is larger than the internal CO_2 release from mineralization ($\gamma \cdot \mathbf{R}_{ox}$=22.7 μmol-C $kg^{-1}\,d^{-1}$), and this difference is balanced by the advective-dispersive $\sum CO_2$ input ($\mathbf{T}_{\sum CO_2}$=18.1 μmol-C $kg^{-1}\,d^{-1}$; positive $\mathbf{T}_{\sum CO_2}$ means larger $\sum CO_2$ inflow than outflow). Accordingly, the upper Schelde estuary emits carbon dioxide from upstream resources. The water is reaerated with oxygen at a rate of $\mathbf{E}_{O_2} = 46.8\,\mu$mol-$O_2$ $kg^{-1}\,d^{-1}$. Oxygen is mostly consumed in oxic mineralization (22.7 μmol-C $kg^{-1}\,d^{-1}$: 49%) and nitrification (16.4 μmol-O_2 $kg^{-1}\,d^{-1}$: 35 %). The budget for oxygen is again closed by advective-dispersive transport, which exports O_2 downstream at a rate of $\mathbf{T}_{O_2}$=7.7 μmol-O_2 $kg^{-1}\,d^{-1}$ (16%).

As noted above, one of the major advantages of the DSA approach is that one can partition $\frac{d[H^+]}{dt}$ (= total change in

Table 15. Steady state baseline values compared with measured values from 2004 (NIOO monitoring data). All quantities except for pH have the unit μ mol kg^{-1}.

quantity	baseline	baseline $+\mathbf{R}_{H_2O}$	baseline $+\mathbf{R}_{H_2O}$ $+\mathbf{R}_{den}$	measured
[OM]	32	32	30	29
[NO_3^-]	340	340	328	322
[O_2]	158	158	159	154
pH	7.70	7.70	7.71	7.70
[$\sum NH_4^+$]	36	36	37	29
[$\sum CO_2$]	6017	6017	6030	
[TA]	5929	5929	5942	

proton concentration) into contributions by different kinetic processes (Eq. 16). At steady state, overall consumption of protons should match overall production. Figure 2 shows that in our baseline simulation, the pH steady state is dominated by the interplay between oxic mineralisation, nitrification and CO_2 air-water exchange. Oxic mineralisation and nitrification respectively produce about 49% and 40% of the protons consumed by CO_2 outgassing. The remaining 11% are the result of advective-dispersive transport ($\sum \mathbf{T}$). The NH_3 exchange with the atmosphere plays a negligible role, as it produces only 0.3% of the protons consumed by CO_2 air-water exchange.

3.2 The influence of H_2O auto-dissociation and denitrification

In the formulation of the model, we deliberately neglected the auto-dissociation of water ($\mathbf{R}_{H_2O}$) and denitrification ($\mathbf{R}_{den}$) to keep the model analysis as simple as possible. A model including H_2O auto-dissociation does not show any differences in steady state results (Table 15, Fig. 2). Accordingly, $\mathbf{R}_{H_2O}$ can be safely omitted.

To check the importance of denitrification, we included the reaction

$$(CH_2O)_\gamma(NH_3)+0.8\,\gamma\ NO_3^-+0.8\,\gamma\ H^+\rightarrow \\ NH_3+\gamma\ CO_2+0.4\,\gamma\ N^2\uparrow+1.4\,\gamma\ H_2O \quad (22)$$

with the kinetic formulation

$$\mathbf{R}_{den} = r_{den}\cdot[OM]\cdot(ks_{O_2}^{inhib}/([O_2]+ks_{O_2}^{inhib})) \\ \cdot([NO_3^-]/([NO_3^-]+ks_{NO_3^-})) \quad (23)$$

with rate constant r_{den}=0.2 d^{-1} (Soetaert and Herman, 1995b), an inhibition constant $ks_{O_2}^{inhib}$=45 μ mol kg^{-1} (Soetaert and Herman, 1995b), and a saturation constant $ks_{NO_3^-}$=22 μ mol kg^{-1} (Regnier et al., 1997). The inclusion of denitrification results in marginal differences in concentrations (Table 15) and does not affect the steady state pH (Fig. 2).

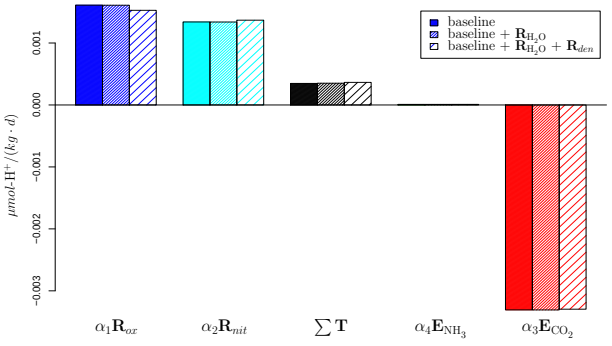

Fig. 2. Partitioning of $\frac{d[H^+]}{dt}$ according to Table D2.

3.3 Three perturbation scenarios

In the perturbation scenarios, the baseline steady state values were imposed as initial conditions.

Scenario A: Decrease in the upstream organic matter loading:

It is estimated that the organic matter loading in the river Schelde will be halved by a new sewage-treatment plant for the city of Brussels, which became operational in 2007. To simulate the impact of this change, we started off from the baseline simulation (values for the year 2004), and decreased the upstream organic matter concentration $[OM]_{up}$ from 50 μmol N kg^{-1} to 25 μmol N kg^{-1} on the fifth day of a 40-day model run. Figure 3 shows the evolution of pH, [TA], [$\sum CO_2$] and [O_2] for this scenario. After about 35 days a new steady state is reached, in line with the 10 day response time-scale of the dominant transport and reaction processes (Table 5). The decrease in OM loading reduces the steady state concentration of organic matter [OM] by 38% (not shown), while oxygen levels increase by 10% and [$\sum CO_2$] levels remain virtually unchanged (slight decrease by 0.3%). Note that the changes occur monotonically. This is different for the total alkalinity, which shows a slight "overshoot" response. TA decreases from 5928.9 μ mol kg^{-1} to a minimum value of 5927.9 μ mol kg^{-1} after 6 days, but then stabilizes at a higher level of 5928.1 μ mol kg^{-1}. This dip in [TA] is explained by a different temporal response of the mineralization, nitrification and transport terms (Fig. 4a). The change in the upstream OM concentration leads to a sharp decline in [OM] in the system, causing $\mathbf{R}_{ox}$ (which produces alkalinity) to drop sharply as well. The nitrification rate $\mathbf{R}_{nit}$ (which consumes alkalinity) however drops less sharply. As a result, temporarily "too much" alkalinity TA is consumed, which results in the observed dip in [TA]. Note that this discussion is only interesting in terms of model internals but is not relevant to the real system, since the changes in [TA] are near or below the measurement accuracy.

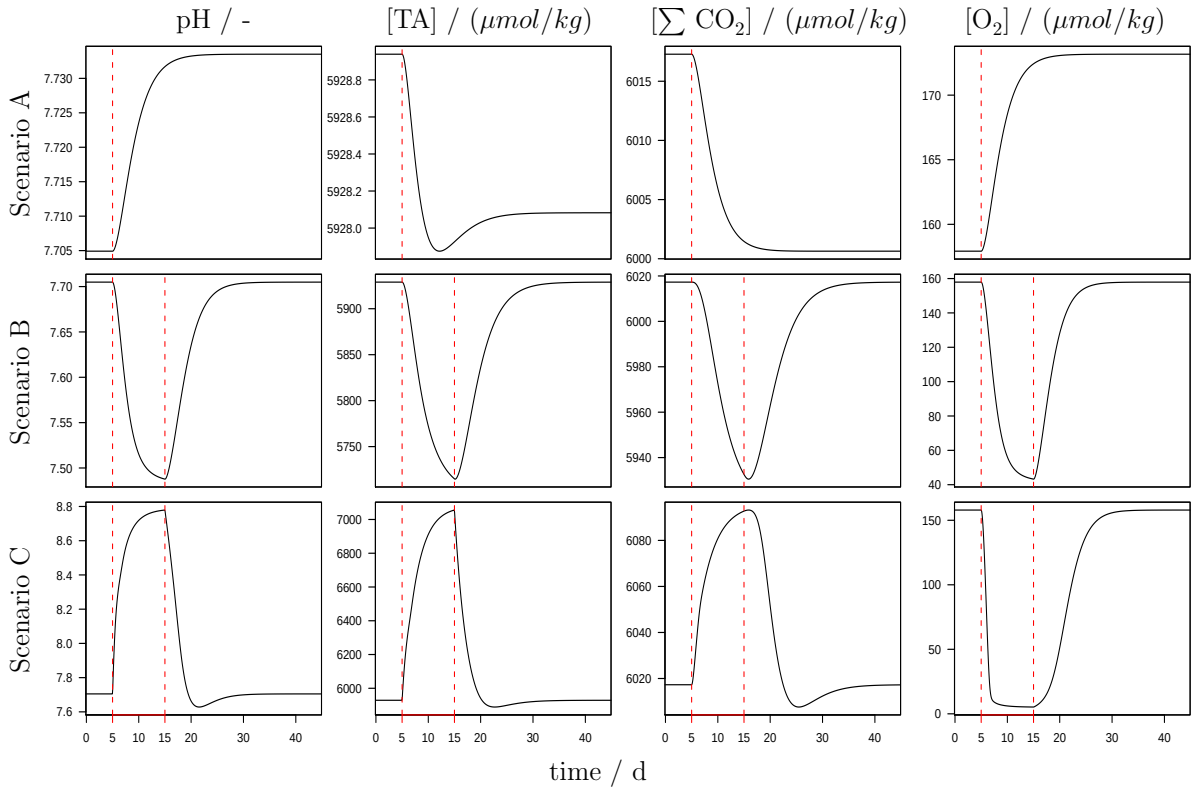

Fig. 3. The pH, [TA], $[\sum CO_2]$ and $[O_2]$ development for the three model scenarios.

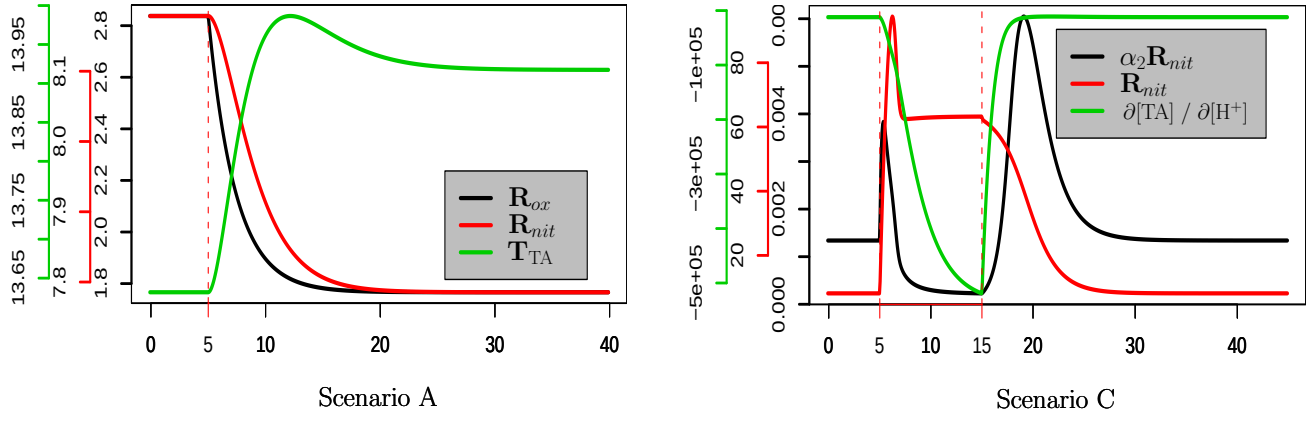

Fig. 4. Key quantities of scenario A and C, all scaled to the plot area.

Also note that the decrease in [TA] (0.8 μ mol kg^{-1}) is much smaller than the corresponding decrease in the DIC concentration (16 μ mol kg^{-1}). This difference is due to the rising pH and the associated re-equilibration within the carbonate system. Although $[\sum CO_2]$ decreases, the CO_2 system dissociates more, due to the pH increase, increasing $[CO_3^{2-}]$. Hence, alkalinity does not follow the decrease in $[\sum CO_2]$ to similar extent (see Table 16).

The new steady state pH of 7.734 is only 0.4% higher than the baseline pH of 7.705. Figure 5 shows that the abrupt decrease in organic matter loading has only a small influence on the pH steady state. The individual contributions of all processes decline, except for the small contribution of advective-diffusive transport. That means the model results are in agreement with intuitive expectations: In a system with less organic matter input, the influence of physical

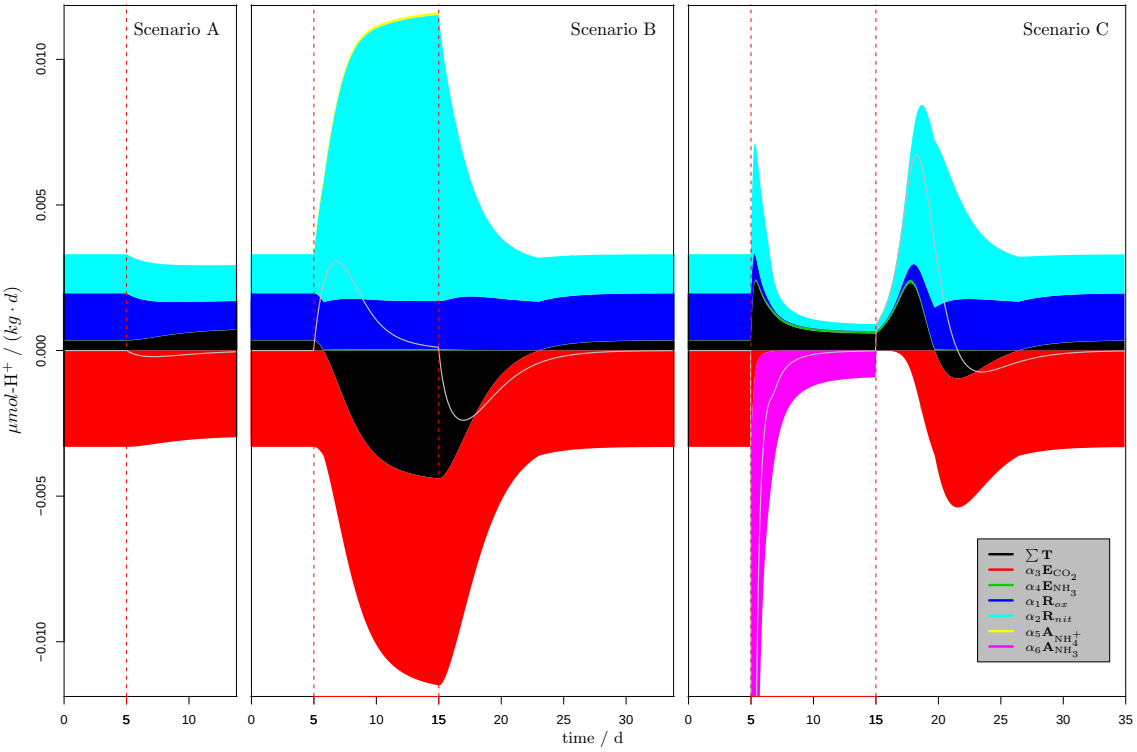

Fig. 5. Budget of $\frac{d[H^+]}{dt}$ for the three model scenarios. The gray line indicates the net $\frac{d[H^+]}{dt}$.

Table 16. The carbonate system before and after the change in upstream organic matter loading (all values in μ mol kg^{-1}).

species	before	after	Δ
$[CO_2]$	164.57	153.8	−10.77
$[HCO_3^-]$	5776.88	5766.0	−10.88
$[CO_3^{2-}]$	75.84	80.85	+5.01

processes on pH increases relative to that of biological processes.

Scenario B: Spill of ammonium nitrate

Due to the presence of the harbour of Antwerp and the surrounding chemical industry, there is potential danger of ship accidents and spills of chemicals into the Schelde estuary. As an example, we consider a spill of ten thousand tons of ammonium-nitrate fertilizer (NH_4^+ NO_3^-; in the molar ratio 1:1). Furthermore, we consider a slowly leaking ship, where the chemicals are released within a period of 10 days (between day 5 and 15 of the simulation). To model this release, we need to include an extra source term for ammonium and nitrate in the MCE's (cf. Table 4).

$$\mathbf{A}_{NH_4^+} = \mathbf{A}_{NO_3^-} = 115\ \mu\text{mol kg}^{-1}\ d^{-1} \tag{24}$$

In a similar manner as for the other kinetic processes, one can derive the influence of the addition of substance X to the system $\mathbf{A}_X$ on the proton change $\frac{d[H^+]}{dt}$, by including $\mathbf{A}_X$ in the MCE's from Table 4. Whereas the addition of nitrate has no effect on the pH, the contribution of $\mathbf{A}_{NH_4^+}$ to $\frac{d[H^+]}{dt}$ has the form as given in Eq. (17), and results in

$$-\left(\frac{\partial[TA]}{\partial[\sum NH_4^+]} \Big/ \frac{\partial[TA]}{\partial[H^+]}\right) \cdot \mathbf{A}_{NH_4^+} := \alpha_5 \cdot \mathbf{A}_{NH_4^+} \tag{25}$$

The second row in Fig. 3 shows the profiles for pH, [TA], $[\sum CO_2]$ and $[O_2]$ for this scenario. Drastic perturbations in the geochemistry of the estuary are simulated during the 10 days of leakage, and during a small period of about 15 days afterwards. The leakage results in a distinct peak in $[\sum NH_4^+]$ (not shown), with values rising by roughly 620% from 36 μ mol kg^{-1} to 260 μ mol kg^{-1}. This is accompanied by a peak in $[NO_3^-]$, rising by 130% from 340 μ mol kg^{-1} to 778 μ mol kg^{-1}, which is due to both the leakage $\mathbf{A}_{NO_3}$ and increased nitrification. Total alkalinity and $[\sum CO_2]$ temporarily drop by 4% and 1% respectively. Oxygen conditions drastically drop from 158 μ mol kg^{-1} to hypoxic conditions at 43 μ mol kg^{-1}, due to a short period of intense nitrification.

pH levels drop by approximately two tenths of a unit from 7.71 to 7.49. Figure 5 shows that this is mainly due to an increase of nitrification, and that the contribution of $\mathbf{A}_{NH_4^+}$

itself is negligible. After 10 days of leakage, dynamic pH equilibrium is almost re-installed, and the proton production of nitrification is compensated by the proton release due to outgassing of CO_2 and from transport. The influence of oxic mineralisation on $\frac{d[H^+]}{dt}$ does not significantly change during the spill, compared to the dominant components. After 10 days, the end of the leakage imposes a new perturbation on the system.

Scenario C: Spill of ammonia

In this sceneario, we investigate a similar ship accident, but now with a spill of ten thousand tons of ammonia (NH_3). The leakage period is identical to the previous case, and the input term for ten thousand tons of ammonia within 10 days becomes

$$\mathbf{A}_{NH_3} = 541\ \mu\text{mol kg}^{-1}\ d^{-1} \quad (26)$$

The contribution of $\mathbf{A}_{NH_3}$ to $\frac{d[H^+]}{dt}$ is

$$\left(\left(1 - \frac{\partial[\text{TA}]}{\partial[\sum \text{NH}_4^+]}\right) \Big/ \frac{\partial[\text{TA}]}{\partial[\text{H}^+]}\right) \cdot \mathbf{A}_{NH_3} := \alpha_6 \cdot \mathbf{A}_{NH_3} \quad (27)$$

Figure 3 shows the profiles for pH, [TA], $[\sum CO_2]$ and $[O_2]$ for this scenario. Again a distinct peak in $[\sum NH_4^+]$ is observed (not shown), with the baseline concentration rising by a factor of 37. This is again accompanied by a 50% increase in $[NO_3^-]$, which is now solely the result of increased nitrification. Total alkalinity and $[\sum CO_2]$ temporarily rise by 20% and 1% respectively. Oxygen concentrations are again greatly reduced (by roughly 97%), now almost reaching full anoxia with a minimum of 5 μ mol kg^{-1}. The oxic mineralisation rate is much lower than in the baseline-simulation due to low oxygen concentrations.

The pH level increases by more than one pH unit from 7.71 to 8.78. Figure 5 shows that this is mainly due to the input of NH_3 into the estuary by the leak. Nitrification initially counters the proton consumption of NH_3 input (via conversion to ammonia), but this effect decreases drastically due to decreasing oxygen levels (cf. the initial steep spike in $\mathbf{R}_{nit}$ shown in the right panel of Fig. 4). The effect of outgassing of ammonia $\mathbf{E}_{NH_3}$ on $\frac{d[H^+]}{dt}$ only becomes important towards the end of the 10 day spill period, when almost steady state conditions are reached. At this point, NH_3 outgassing and subsequent dissociation of ammonium (as the equilibrium state changes due to Le Chatelier's principle) balance, together with the effects of nitrification and advective-dispersive transport, the proton consumption of $\mathbf{A}_{NH_3}$ and subsequent association of ammonium. When the leakage is stopped, the system returns to the pre-leakage state within a matter of 15 days. There is however a dip in pH and alkalinity before baseline values are attained again. Immediately after the leakage stops, there is still a lot of $\sum NH_4^+$ in the system, which is further nitrified. The effects of CO_2 outgassing and advective-dispersive transport (which changes sign again) compensate for the proton production associated with nitrification. However, this compensation occurs with a certain time lag, creating the dip in pH after the initial spike.

The net absolute values of proton consumption or production of all processes decreases during the 10 day spill period due to an increase in the absolute value of the buffering capacity $\frac{\partial[\text{TA}]}{\partial[\text{H}^+]}$, which changes from $-0.165\ 10^5$ to $-5.15\ 10^5$ (Fig. 4). It can be noted that in our modelled pH range the absolute value of $\frac{\partial[\text{TA}]}{\partial[\text{H}^+]}$ increases with increasing pH. This leads to the conclusion that the higher the pH of the system, the closer to zero the influences of processes on $\frac{d[H^+]}{dt}$.

Table 17. Summary of our pH modeling approach.

pH modeling in 10 steps
1 Formulation of the model question.
2 Formulation of the conceptual model.
3 Constraining the model pH range - selection of acid-base reactions.
4 Writing down a MCE for all species whose concentrations are influenced by modeled processes. The system is now solvable with the **full kinetic approach (FKA)**.
5 Partitioning the modeled process into kinetic and equilibrium processes according to their timescales and defining kinetic expressions for kinetic processes.
6 Mathematically closing the system by formulating the mass action laws of the equilibrium processes.
7 Transforming the system into the canonical form: reformulating it into an implicit DAE system without any purely algebraic variables. The system is now solvable with the **full numerical approach (FNA)**.
8 Introducing the equilibrium invariants to convert the differential equations of the DAE into explicit ODEs.
9 Reformulating the algebraic part of the DAE to explicitly express all equilibrium species as functions of $[H^+]$ and equilibrium invariants. The system is now solvable with the **operator splitting approach (OSA)**.
10 Reformulating the system according to the **direct substitution approach (DSA)**: substitute the expression for $\frac{d[\text{TA}]}{dt}$ by an expression for $\frac{d[H^+]}{dt}$ to get rid of the AE systems nonlinearity in an unknown variable. The expression for $\frac{d[H^+]}{dt}$ can be partitioned such that the influences of modeled kinetic processes onto $\frac{d[H^+]}{dt}$ can be quantified.

Table 18. CPU time in miliseconds for one model run of all mentioned solution approaches and scenarios. Values are averages of 1000 runs each. All approaches are integrated with DASSL to be comparable. The model output generated with the five approaches is identical. The FKA is implemented according to solution method 1b. The OSA (3a) has been implemented using the Newton-Raphson root finding procedure. Constant K^*'s are assumed for all approaches. The benchmarking has been done on an Intel® Pentium® 4 CPU with 3 GHz and 1 GB RAM, running Microsoft Windows XP Professional, Version 2002, SP2. The compiling has been done with Compaq Visual Fortran Professional Edition 6.6.0. Please note that the computational advantage of OSA (3b) and DSA over FKA, FNA and OSA (3b) is expected to me more prominent for more complex systems. However, a detailed theoretical runtime analysis of all methods is beyond the scope of this paper.

scenario	FKA(1b)	FNA	OSA (3a)	OSA (3b)	DSA
baseline simulation	70	63	48	43	43
A	74	69	53	48	48
B	77	72	58	50	50
C	80	74	59	51	52

4 Discussion

4.1 A consistent framework for pH model generation

The overall result of our work is a general recipe for pH model formulation, consisting of 10 separate steps (Table 17), which we clarified by means of an example. We have identified four main solution techniques (FKA, FNA, OSA, DSA), which all enable the solution of the non-steady-state pH problem. These four solution techniques are connected by three consecutive mathematical transformations of the pH problem. Although it requires an initial investment, such a reformulation effort has multiple advantages, both practically, in terms of more efficient simulations, as well as theoretically, in terms of improved physical and chemical insight into the problem.

Along the course of the mathematical reformulations two approximations have been made.

1) To make the transition from the FKA to the FNA (the transformation into the canonical form) the local equilibrium assumption has been applied. As mentioned earlier, this approximation generally has no influence on the results of models of macroscopic systems.

2) To reformulate the system into a form solvable by the DSA, the K^*'s of the system are assumed constant. This has been done for didactical reasons to keep the mathematical expressions simple. This, however, is no limitation: variable K^*'s can be integrated into the DSA as well.

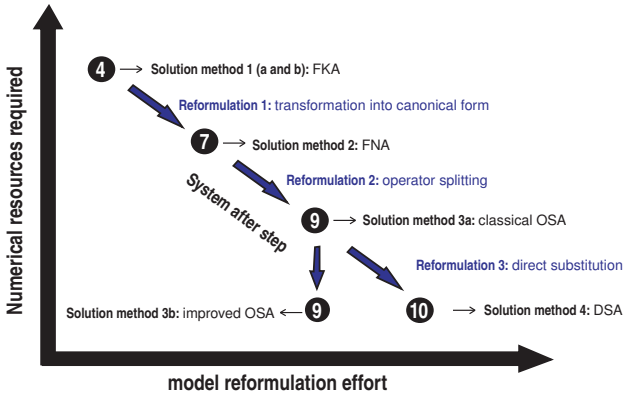

Fig. 6. The trade-off between numerical resource requirement and model reformulation effort.

Although these approximations have been made, our four main solution methods are still different mathematical formulations of the same model yielding the same results: both approximations can also be made from the very beginning. The local equilibrium assumption can be included into the FKA (solution method 1b) and the K^*'s can be assumed constant for all approaches. What remains is a chain of mathematical transformations, with no further approximations involved.

As shown in Table 18 and in Fig. 6, even if the local equilibrium assumption and constant K^*'s are applied to all approaches, there is a clear trade-off between reformulation effort and the numerical resources required. The more the pH problem is initially reformulated, the less computation time is spent on actual pH simulations afterwards. The reformulations transform the pH problem into a more elegant mathematical form, and only require a one-time investment during the model generation process. Accordingly, when doing multiple simulations as in a sensitivity analysis, the initial time investment in reformulation is likely to pay off very rapidly. Although, in terms of computational performance, the improved OSA and the DSA are comparable, the DSA additionally allows for the quantification of the influences of kinetically modelled processes on the pH. These influences are calculated against the background of re-equilibration of the system due to a set of acid-base equilibria.

The DSA approach thus comes out as the most powerful procedure to tackle pH models. However, in a system where the dissociation constants (K^*'s) cannot be assumed constant, the influence of temperature, salinity and pressure on the dissociation constants has to be incorporated into the DSA. This has been deliberately omitted from this paper for didactical reasons.

4.2 Comparison with previous approaches

Past pH modeling approaches can be equated to one of the four solution methods in Fig. 6. The most basic approach,

the Full Kinetic Approach (FKA) has only been implemented sporadically (Steefel and MacQuarrie, 1996; Zeebe, 2007), because of the numerical stiffness of the obtained equation systems (solution method 1a and 1b), and the need to obtain parameters that are not very well constrained (forward and backward rates of acid-base reactions in solution method 1a). After one reformulation step termed the transformation into canonical form (DiToro, 1976; Lichtner, 1996; Steefel and MacQuarrie, 1996; Chilakapati et al., 1998; Saaltink et al., 1998; Meysman, 2001) based on an idea first put forward by Aris and Mah (1963), one can implement the Full Numerical Approach (FNA), which involves a direct numerical solution of the resulting differential algebraic equation system. Steefel and MacQuarrie (1996) list a number of packages, including DASSL (Petzold, 1982), capable of solving a system according to the FNA. Gehlen et al. (1999) applied this solution technique in a relatively simple pH problem (4 acid-base reactions) to study the distribution of stable carbon isotopes in the pore water of deep sea sediments. We are not aware of FNA applications with realistic "field-type" reaction sets (including 10 or more acid-base reactions). In these situations, FNA simulations are expected to require significant computational resources.

The demanding computations of the FNA can be avoided by means of a second reformulation, via the introduction of equilibrium invariants. This reformulation allows uncoupling the differential and algebraic part of the DAE system and solving them independently. The resulting approach is termed operator splitting (OSA, steps 8 and 9). Regnier et al. (1997) used the OSA to model pH along an estuarine gradient, Marinelli and Boudreau (1996) used it to study the pH in irrigated anoxic coastal sediments, and Follows et al. (1996) used the OSA to investigate the carbonate system in the water column of the North Atlantic. Besides pointing out different varieties of the FNA, Chilakapati et al. (1998) also applied the OSA to simple groundwater problems. While not explicitly reformulating the system, Boudreau (1987), Boudreau and Canfield (1988), Boudreau (1991), Boudreau and Canfield (1993), and Boudreau (1996a) (the CANDI model) used the notion of dividing the reaction set into kinetic reactions and equilibrium reactions. Imposed equilibrium invariants were then used to simulate steady state pH profiles of aquatic sediments. Therefore, these approaches can be viewed as predecessors of the OSA. Although equilibrium invariants were not explicitly defined, Wang and Van Cappellen (1996) (the STEADYSED1 model) uncoupled the DE and the AE part of the DAE system and solved them separately, making their approach a quasi OSA. In a detailed methodological study on pH modeling, Luff et al. (2001) examined different variations of the OSA: three different possibilities for the algebraic equation part of the DAE system were introduced.

As noted above, there are two major disadvantages associated with the classical OSA approach (1) the equilibration step requires a numerical solution, which makes the OSA computationally intense, and (2) the OSA does not allow quantifying the influence of different processes on $\frac{d[H^+]}{dt}$. The numerical solution step can be eliminated using the improved OSA put forward by Follows et al. (2006), but it still lacks the possibility of assessing influences of kinetically modelled processes on the pH.

The two problems of the OSA vanish after a third reformulation, which leads to the Direct Substitution Approach (DSA). Therefore, we consider the DSA approach to be the most elegant and promising pH modeling procedure, especially if knowledge of the influences of modelled processes on the pH is desired. If this knowledge is not desired, the improved OSA according to Follows et al. (2006) might be the method of choice, since the third reformulation of the system (step 10) is not necessary. In the DSA, the differential equation for total alkalinity is replaced by a differential equation for the proton concentration, which enables a direct analytical solution of the equilibration step. The most important advantage is that the change in $[H^+]$ can be partitioned into contributions by different processes, and hence, the influence of processes on pH can be directly assessed (as discussed further below).

Although applying the DSA, Meysman et al. (2003) (the MEDIA modelling environment) did not make use of its capability of assessing influences of processes on the pH.

In recent years two other studies have employed DSA-like approaches to assess influences of processes on the pH. Yet the way these methods were derived is not fully clear as the presentations are prone to internal inconsistencies.

The approach of Jourabchi et al. (2005) is situated somewhere between the DSA and the FNA. As a by-product in calculating stoichiometric coefficients for equilibrium species, Jourabchi et al. (2005) calculated a rate of change of protons over time for a given modelled process, starting from the total derivative of total alkalinity. However, these rates do not add up to a total rate of change since the effect of transport is not made explicit. Direct proton transport is even omitted as they remove the mass conservation equation for protons to cope with an overdetermined equation system, which introduces an error. Their equation system was subsequently solved with a numerical solver that depended on steady state conditions of the system. This means dynamic pH simulations are not possible. Total quantities like total alkalinity were imposed and not consistently derived. Subsequently, [TA] was used in a way that in some points contradicted Dickson's (Dickson, 1981) notion of [TA].

Soetaert et al. (2007) also made a step towards a DSA, but fell short of deriving a total rate of change of protons. They needed to invoke several ad-hoc assumptions and concepts like the mean and total charge of postulated total quantities to arrive at formulae for the influence of modeled processes on the pH. These formulae did not add up to a total rate of change of protons over time, because no transport terms were included. This means that modeling the pH of a real system containing several processes at the same time was not possible.

4.3 Implicit assumptions

The subsequent reformulations of the system (Fig. 6) yield more insight into the physical, chemical, and mathematical structure of the pH problem. By delineating all steps of the model generation process explicitly, one achieves a high level of model transparency. Typically, past treatments do not explicitly list all assumptions and decisions made during the model generation process. This practice has led to the introduction of unnecessary assumptions and constraints, as well as inconsistently employed concepts.

A first difference between our approach and past treatments is that we do not need an a priori definition of alkalinity. In other words, in our treatment, the way alkalinity is defined in terms of the other chemical species follows directly from the model reformulation. As shown above, alkalinity is one of the equilibrium invariants (like total inorganic carbon and total ammonium). These equilibrium invariants emerge after the transformation of the pH problem into the canonical form and are equivalent to the mole balance equations of Morel's *components* (Morel and Hering, 1993) as well as to DiToro's *reaction invariants* (DiToro, 1976) of the system. Similar quantities appear in Boudreau (1987), Boudreau and Canfield (1988), Boudreau (1991), and Boudreau and Canfield (1993). Equilibrium invariants, and hence alkalinity, are quantities that are conservative with respect to equilibrium reactions. The exact form of alkalinity depends on the chosen set of equilibrium reactions, and hence, it is dependent on the chosen pH range of the model and the chosen time scale of the model. This practice ensures (1) consistency between the definition of total alkalinity and the model, and (2) the correct stoichiometric coefficients in the MCE for total alkalinity (cf. Eq. (6) in Table 12).

A second difference is that we do not need the assumption of electroneutrality. Approaches like e.g. Luff's (Luff et al., 2001) charge balance approach, or the CANDI model (Boudreau, 1996a) implicitly assume electroneutrality of the solution. They use a measure of total charge (including conservative ions like Na^+), which is assumed to be zero, to close their equation systems[5]. Although sometimes wrongly termed so (e.g. Boudreau, 1991; Follows et al., 1996, 2006), total alkalinity is not a charge balance, but a proton balance. It expresses the excess of proton equivalents (protons and proton donors) to proton acceptors (Dickson, 1981; Wolf-Gladrow et al., 2007). This means that if, for example, NO_3^- is assumed not to react with H^+ in the pH range that is modelled, the concentration of nitrate does not have any influence on total alkalinity, although it is an integral part of the total charge balance of the solution. By consistently using total alkalinity instead of a charge balance, concentrations of conservative ions do not enter the pH calculation.

Furthermore, as mentioned above, our approach directly provides the stoichiometric coefficients for total alkalinity for all kinetic processes. Although these coefficients are not obvious from the definition of [TA], as all component concentrations are influenced by equilibrium reactions, our model generation procedure unambiguously provides them. To this end, a reformulation of the expression of [TA] into the "explicit conservative total alkalinity", which requires electroneutrality of the solution, as put forward by Wolf-Gladrow et al. (2007), is not needed.

4.4 Assessing the influence of processes on pH

In a system that contains slow kinetic processes (slow kinetic biogeochemical reactions, but also transport) and fast equilibrium processes, the independent drivers of the system, that means the factors that determine the temporal evolution of the state of the system, are only the slow kinetic processes. When adopting local equilibrium, the net rates of the equilibrium processes become dependent on the rates of the kinetic processes.

Therefore it is of interest to assess the influences of the slow kinetic processes on the pH. To do so, one needs an explicit formulation for $\frac{d[H^+]}{dt}$ which can be partitioned into explicit contributions by each of these different slow kinetic processes.

Two of our main solution approaches provide an explicit formulation for $\frac{d[H^+]}{dt}$: the FKA and the DSA. However, the formulation for $\frac{d[H^+]}{dt}$ as obtained by the FKA contains terms contributed by equilibrium reactions. These equilibrium terms implicitly contain the influences of all slow kinetic processes that influence the reactants and products of the equilibrium reaction in question. Therefore, the formulation for $\frac{d[H^+]}{dt}$ as obtained by the FKA cannot be partitioned into explicit separate terms for the influences of all slow kinetic processes on the pH.

Exactly there lies the most important advantage of the DSA method as it provides an explicit partitioning of the formulation for $\frac{d[H^+]}{dt}$ into the influences of all slow kinetic processes on the pH against the background of buffering by an equilibrium reaction system.

Unlike Soetaert et al. (2007) and Jourabchi et al. (2005), in our DSA we obtain an explicit formulation for the contribution of all kinetic processes to $\frac{d[H^+]}{dt}$, including transport. This enables a deeper understanding of how pH steady state is attained, and what processes exactly are responsible for a pH change upon disturbance of the system. This is clearly illustrated in our disturbance scenarios for a simple estuarine system.

Furthermore, the buffering capacity of the solution $\frac{\partial[TA]}{\partial[H^+]}$ is identified as an important and central quantity, as it modulates the influence of all processes on the pH. A process with

[5]Similar to our approach, the approach put forward by Soetaert et al. (2007) does not depend on the electroneutrality of the solution, although the names of the quantities they use suggest so. They sometimes require "electroneutrality" of both sides of a reaction equation, but this is not the same as electroneutrality of the solution and should be better termed "reactional charge conservation".

the same rate, can have a different influence on the pH depending on the state of the system, as represented by $\frac{\partial[\mathrm{TA}]}{\partial[\mathrm{H}^+]}$. Our disturbance scenario C shows that it is possible that in certain circumstances, although process rates increase, the absolute values of influences of processes on $\frac{d[\mathrm{H}^+]}{dt}$ can decrease, since the absolute value of $\frac{\partial[\mathrm{TA}]}{\partial[\mathrm{H}^+]}$ increases due to an increased pH. Figuratively this can be explained by the fact that a higher pH means less free protons in solution. Therefore, the amount of protons affected by a certain process is decreased. $\frac{\partial[\mathrm{TA}]}{\partial[\mathrm{H}^+]}$ is a measure for this condition.

5 Conclusions

In the present paper, we systematically and consistently derived a succession of methods to model pH, making every step of the model generation process explicit. The chemical structure of the model was used for sucessive reformulations until fast and elegant numerical solutions were possible. Existing pH modelling approaches were identified within this framework and advantages and drawbacks were pointed out. Definitions for summed quantities and the influence of all modelled processes on them where derived from the model. With the DSA the influence of modelled kinetic processes on the pH can be quantified.

Appendix A

Criterion for exclusion of acid-base reactions

To decide whether or not a certain acid-base reaction will be included in the model, we calculate a quantity ϵ for every acid-base dissociation step. Polyprotic acids are treated as a set of monoprotic acids, considering each dissociation step independently. The total concentration $[\sum \mathrm{A}]$ considered for each dissociation step is assumed equal to the total concentration of the polyprotic acid (For example, for both dissociation steps of CO_2 in seawater, the total concentration is assumed to be $[\sum \mathrm{CO_2}]$). Since this overestimates the error, it is a conservative practice. The quantity ϵ represents the amount of protons δ (concentration offset) ignored by neglecting the reaction in question, in percent of the average [TA] of the modeled system.

$$\epsilon = (\delta/[\mathrm{TA}]) \cdot 100 \tag{A1}$$

Reactions with an ϵ value below the desired error threshold percentage ν can be neglected.

Consider the acid in question to be HA with pK^*_A and a total concentation of $[\sum \mathrm{A}]$. Consider further a designated pH range of $\mathrm{pH_{low}} \leq \mathrm{pH} \leq \mathrm{pH_{up}}$. To calculate δ, we distinguish three cases (Fig. A1)

1) $\mathrm{pH}_{low} < \mathrm{pK}^*_\mathrm{A} < \mathrm{pH_{up}}$: Neglecting the dissociation reaction in this case means not including any species of the respective acid-base system in the model. δ can be as high as the total concentration of the acid:

$$\delta = [\sum \mathrm{A}] \tag{A2}$$

2) $\mathrm{pK}^*_\mathrm{A} \leq \mathrm{pH_{low}}$: Neglecting the dissociation reaction in this case means that the acid is assumed to be fully dissociated. δ can be as high as the concentration of the undissociated form of the acid at the lower boundary of the pH range $[\mathrm{HA}]_{\mathrm{low}}$. One can estimate an upper limit for $[\mathrm{HA}]_{\mathrm{low}}$:

$$\delta = 10^{\left(\mathrm{pK}^*_\mathrm{A} - \mathrm{pH_{low}}\right)} \cdot [\sum \mathrm{A}] \geq [\mathrm{HA}]_{\mathrm{low}} \tag{A3}$$

3) $\mathrm{pH_{up}} \leq \mathrm{pK}^*_\mathrm{A}$: Neglecting the dissociation reaction in this case means that the acid is assumed to be fully undissociated. δ can be as high as the concentration of the corresponding base at the upper boundary of the pH range $[\mathrm{A}^-]_{\mathrm{up}}$. One can estimate an upper limit for $[\mathrm{A}^-]_{\mathrm{up}}$:

$$\delta = 10^{\left(\mathrm{pH_{up}} - \mathrm{pK}^*_\mathrm{A}\right)} \cdot [\sum \mathrm{A}] \geq [\mathrm{A}^-]_{\mathrm{up}} \tag{A4}$$

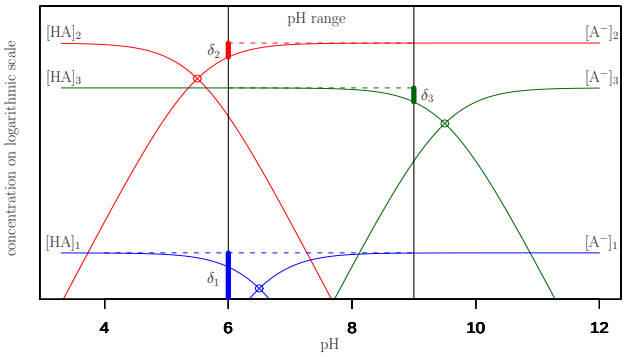

Fig. A1. Bjerrum plot for three different cases to calculate δ for acid-base dissociation reactions. Locations of pK^*_A are indicated with circles.

ϵ values for our reactions, model pH range and [TA] are given in Table 2.

Appendix B

Transformation into canonical form

Having partitioned the processes into n_{kp} kinetic and n_{ep} equilibrium processes, the mass-balance Eq. (1), can be written in matrix notation for all n_{es} equilibrium species

$$\mathbf{I} \times \frac{d[C]}{dt} = \boldsymbol{\nu}_{\mathrm{kin}} \times \boldsymbol{R}_{\mathrm{kin}} + \boldsymbol{\nu}_{\mathrm{eq}} \times \boldsymbol{R}_{\mathrm{eq}} \tag{B1}$$

where $\mathbf{I}$ is the $n_{es} \times n_{es}$ identity matrix, $\frac{d[C]}{dt}$ is a vector with time derivatives of all n_{es} species, $\boldsymbol{\nu}_{\mathrm{eq}}$ is the $n_{ep} \times n_{es}$

stoichiometric matrix for the equilibrium reactions, $\boldsymbol{\nu}_{\mathrm{kin}}$ is the $n_{kp}\times n_{es}$ stoichiometric matrix for the influence of the kinetic reactions on the equilibrium species, $\boldsymbol{R}_{\mathrm{kin}}$ is the vector of the kinetic reactions, and $\boldsymbol{R}_{\mathrm{eq}}$ is the vector of the equilibrium reactions.

The goal is to find a linear transformation $\mathbf{P}$ such that

$$\mathbf{P}\times\frac{d[C]}{dt}=\mathbf{P}\times\boldsymbol{\nu}_{\mathrm{kin}}\times\boldsymbol{R}_{\mathrm{kin}}+\mathbf{P}\times\boldsymbol{\nu}_{\mathrm{eq}}\times\boldsymbol{R}_{\mathrm{eq}} \tag{B2}$$

$\mathbf{P}$ can be constructed by performing a Gauss-Jordan elimination applied to the matrix $\boldsymbol{\nu}_{\mathrm{eq}}$ (By adequate selection of the row operations during the Gauss-Jordan elimination, a subset of Dickson's total alkalinity (Dickson, 1981) as well as a subset of any other desired similar quantity like Soetaert's "sum of excess negative charges" (Soetaert et al., 2007) can be obtained as an equilibrium invariant).

The result of this operation is the *reduced row-echelon* form of $\boldsymbol{\nu}_{\mathrm{eq}}$, which is also known as the *row canonical form*. Equation (B3) gives $\mathbf{P}$, $\boldsymbol{\nu}_{\mathrm{eq}}$ and the reduced row-echelon form of $\boldsymbol{\nu}_{\mathrm{eq}}$ of our system.

$$\mathbf{P}\times\boldsymbol{\nu}_{\mathrm{eq}}=\begin{pmatrix}0&1&1&0&0&0\\0&0&1&0&0&0\\0&0&0&0&1&0\\1&1&1&0&0&0\\0&0&0&1&1&0\\0&1&2&0&1&-1\end{pmatrix}\times\begin{pmatrix}-1&0&0\\1&-1&0\\0&1&0\\0&0&-1\\0&0&1\\1&1&1\end{pmatrix}=\begin{pmatrix}1&0&0\\0&1&0\\0&0&1\\0&0&0\\0&0&0\\0&0&0\end{pmatrix} \tag{B3}$$

Expanding Eq. (B2) and plugging in P leads to:

$$\begin{pmatrix}0&1&1&0&0&0\\0&0&1&0&0&0\\0&0&0&0&1&0\\1&1&1&0&0&0\\0&0&0&1&1&0\\0&1&2&0&1&-1\end{pmatrix}\times\begin{pmatrix}\frac{d[CO_2]}{dt}\\\frac{d[HCO_3^-]}{dt}\\\frac{d[CO_3^{2-}]}{dt}\\\frac{d[NH_4^+]}{dt}\\\frac{d[NH_3]}{dt}\\\frac{d[H^+]}{dt}\end{pmatrix}= \tag{B4}$$

$$\begin{pmatrix}0&1&1&0&0&0\\0&0&1&0&0&0\\0&0&0&0&1&0\\1&1&1&0&0&0\\0&0&0&1&1&0\\0&1&2&0&1&-1\end{pmatrix}\times\begin{pmatrix}1&0&0&0&0&0&\gamma&0&1&0\\0&1&0&0&0&0&0&0&0&0\\0&0&1&0&0&0&0&0&0&0\\0&0&0&1&0&0&0&0&0&0\\0&0&0&0&1&0&1&-1&0&1\\0&0&0&0&0&1&0&1&0&0\end{pmatrix}\times\begin{pmatrix}\mathbf{T}_{CO_2}\\\mathbf{T}_{HCO_3^-}\\\mathbf{T}_{CO_3^{2-}}\\\mathbf{T}_{NH_4^+}\\\mathbf{T}_{NH_3}\\\mathbf{T}_{H^+}\\\mathbf{R}_{ox}\\\mathbf{R}_{nit}\\\mathbf{E}_{CO_2}\\\mathbf{E}_{NH_3}\end{pmatrix}+\begin{pmatrix}1&0&0\\0&1&0\\0&0&1\\0&0&0\\0&0&0\\0&0&0\end{pmatrix}\times\begin{pmatrix}\mathbf{R}^{dis}_{CO_2}\\\mathbf{R}^{dis}_{HCO_3^-}\\\mathbf{R}^{dis}_{NH_4^+}\end{pmatrix}$$

$$=\begin{pmatrix}0&1&1&0&0&0&0&0&0&0\\0&0&1&0&0&0&0&0&0&0\\0&0&0&0&1&0&1&-1&0&1\\1&1&1&0&0&0&\gamma&0&1&0\\0&0&0&1&1&0&1&-1&0&1\\0&1&2&0&1&-1&1&-2&0&1\end{pmatrix}\times\begin{pmatrix}\mathbf{T}_{CO_2}\\\mathbf{T}_{HCO_3^-}\\\mathbf{T}_{CO_3^{2-}}\\\mathbf{T}_{NH_4^+}\\\mathbf{T}_{NH_3}\\\mathbf{T}_{H^+}\\\mathbf{R}_{ox}\\\mathbf{R}_{nit}\\\mathbf{E}_{CO_2}\\\mathbf{E}_{NH_3}\end{pmatrix}+\begin{pmatrix}1&0&0\\0&1&0\\0&0&1\\0&0&0\\0&0&0\\0&0&0\end{pmatrix}\times\begin{pmatrix}\mathbf{R}^{dis}_{CO_2}\\\mathbf{R}^{dis}_{HCO_3^-}\\\mathbf{R}^{dis}_{NH_4^+}\end{pmatrix}$$

Expanding further and solving the first three equations for the equilibrium reaction rates results in the equation system:

$$\begin{aligned}
\mathbf{R}^{dis}_{CO_2} &= \frac{d[HCO_3^-]}{dt}+\frac{d[CO_3^{2-}]}{dt}-\mathbf{T}_{HCO_3^-}-\mathbf{T}_{CO_3^{2-}}\\
\mathbf{R}^{dis}_{HCO_3^-} &= \frac{d[CO_3^{2-}]}{dt}-\mathbf{T}_{CO_3^{2-}}\\
\mathbf{R}^{dis}_{NH_4^+} &= \frac{d[NH_3]}{dt}-\mathbf{T}_{NH_3}-\mathbf{R}_{ox}+\mathbf{R}_{nit}-\mathbf{E}_{NH_3}\\
\frac{d[CO_2]}{dt}+\frac{d[CO_3^{2-}]}{dt}+\frac{d[HCO_3^-]}{dt} &= \mathbf{T}_{CO_2}+\mathbf{T}_{HCO_3^-}+\mathbf{T}_{CO_3^{2-}}+\gamma\mathbf{R}_{ox}+\mathbf{E}_{CO_2}\\
\frac{d[NH_4^+]}{dt}+\frac{d[NH_3]}{dt} &= \mathbf{R}_{ox}-\mathbf{R}_{nit}+\mathbf{E}_{NH_3}\\
\frac{d[HCO_3^-]}{dt}+2\frac{d[CO_3^{2-}]}{dt}+\frac{d[NH_3]}{dt}-\frac{d[H^+]}{dt} &= \mathbf{T}_{HCO_3^-}+2\mathbf{T}_{CO_3^{2-}}+\mathbf{T}_{NH_3}-\mathbf{T}_{H^+}+\mathbf{R}_{ox}-2\mathbf{R}^{nit}+\mathbf{E}_{NH_3}
\end{aligned}$$

This system is a replacement for the e_s differential MCE's of the equilibrium species as given in Table 4. The first three equations can be removed reducing both the number of unknowns and the number of equations. The removed equations can be used to calculate the unknown net equilibrium reaction rates $\mathbf{R}^{dis}_{CO_2}$, $\mathbf{R}^{dis}_{HCO_3^-}$, and $\mathbf{R}^{dis}_{NH_4^+}$ as output variables of the model.

Appendix C

Reformulation of the AE system

The algebraic equations of the DAE system including the substituted equilibrium invariants reads:

$$0=[H^+][HCO_3^-]-K^*_{CO_2}[CO_2] \tag{C1}$$

$$0=[H^+][CO_3^{2-}]-K^*_{HCO_3^-}[HCO_3^-] \tag{C2}$$

$$0=[H^+][NH_3]-K^*_{NH_4^+}[NH_4^+] \tag{C3}$$

$$[\textstyle\sum CO_2]=[CO_2]+[HCO_3^-]+[CO_3^{2-}] \tag{C4}$$

$$[\textstyle\sum NH_4^+]f=[NH_3]+[NH_4^+] \tag{C5}$$

$$[TA]=[HCO_3^-]+2[CO_3^{2-}]+[NH_3]-[H^+] \tag{C6}$$

We can solve Eqs. (C1) to (C3) for concentrations of equilibrium species to obtain:

$$[HCO_3^-]=\frac{K^*_{CO_2}[CO_2]}{[H^+]} \tag{C7}$$

$$[CO_2]=\frac{[H^+][HCO_3^-]}{K^*_{HCO_3^-}} \tag{C8}$$

$$[CO_3^{2-}]=\frac{K^*_{HCO_3^-}[HCO_3^-]}{[H^+]} \tag{C9}$$

$$[HCO_3^-]=\frac{[H^+][CO_3^{2-}]}{K^*_{HCO_3^-}} \tag{C10}$$

$$[NH_3] = \frac{K^*_{NH_4^+}[NH_4^+]}{[H^+]} \quad \text{(C11)}$$

$$[NH_4^+] = \frac{[H^+][NH_3]}{K^*_{NH_4^+}} \quad \text{(C12)}$$

Adding up Eqs. (C7), (C8) and (C9), as well as (C11) and (C12) yields:

$$[\sum CO_2] = \frac{K^*_{CO_2}[CO_2]}{[H^+]} + \frac{[H^+][HCO_3^-]}{K^*_{HCO_3^-}} + \frac{K^*_{HCO_3^-}[HCO_3^-]}{[H^+]} \quad \text{(C13)}$$

$$[\sum NH_4^+] = \frac{K^*_{NH_4^+}[NH_4^+]}{[H^+]} + \frac{[H^+][NH_3]}{K^*_{NH_4^+}} \quad \text{(C14)}$$

Plugging Eq. (C7) into (C13) and solving for $[CO_2]$, plugging Eq. (C8) into (C13) and solving for $[HCO_3^-]$, plugging first (C8) and then (C10) into (C13) and solving for $[CO_3^{2-}]$, plugging (C11) into (C14) and solving for $[NH_4^+]$, plugging (C12) into (C14) and solving for $[NH_3]$ results in the reformulated form of the algebraic equation system as given in Table 12.

Appendix D

Additional formulae

D1 Analytical partial derivatives in Eq. (15)

Analytically deriving the equations in Table 12, the equations in Table D1 can be obtained.

D2 Coefficients for the rearrangement of the equation for $\frac{d[H^+]}{dt}$ (Eq. 16)

Table D2 gives the coefficients for the partitioning of Eq. (16) into contributions by different kinetically modelled processes.

Table D1. Analytical partial derivatives in Eq. (15).

$$\left.\frac{\partial[TA]}{\partial[\sum CO_2]}\right|_{h,n} = \frac{K^*_{CO_2}[H^+]}{[H^+]^2 + K^*_{CO_2}[H^+] + K^*_{CO_2}K^*_{HCO_3^-}} + 2\left(\frac{K^*_{CO_2}K^*_{HCO_3^-}}{[H^+]^2 + K^*_{CO_2}[H^+] + K^*_{CO_2}K^*_{HCO_3^-}}\right)$$

$$\left.\frac{\partial[TA]}{\partial[\sum NH_4^+]}\right|_{h,c} = \frac{K^*_{NH_4^+}}{[H^+] + K^*_{NH_4^+}}$$

$$\left.\frac{\partial[TA]}{\partial[H^+]}\right|_{c,n} = \frac{\partial[HCO_3^-]}{\partial[H^+]} + 2\frac{\partial[CO_3^{2-}]}{\partial[H^+]} + \frac{\partial[NH_3]}{\partial[H^+]} - \frac{\partial[H^+]}{\partial[H^+]}$$

$$\frac{\partial[HCO_3^-]}{\partial[H^+]} = \left(\frac{K^*_{CO_2}}{[H^+]K^*_{CO_2} + K^*_{CO_2}K^*_{HCO_3^-} + [H^+]^2} - \frac{[H^+]K^*_{CO_2}\left(2[H^+] + K^*_{CO_2}\right)}{\left([H^+]K^*_{CO_2} + K^*_{CO_2}K^*_{HCO_3^-} + [H^+]^2\right)^2}\right)[\sum CO_2]$$

$$\frac{\partial[CO_3^{2-}]}{\partial[H^+]} = -\frac{K^*_{CO_2}K^*_{HCO_3^-}\left(2[H^+] + K^*_{CO_2}\right)}{\left([H^+]K^*_{CO_2} + K^*_{CO_2}K^*_{HCO_3^-} + [H^+]^2\right)^2}[\sum CO_2]$$

$$\frac{\partial[NH_3]}{\partial[H^+]} = -\frac{K^*_{NH_4^+}}{[H^+]^2 + 2[H^+]K^*_{NH_4^+} + (K^*_{NH_4^+})^2}[\sum NH_4^+]$$

$$\frac{\partial[H^+]}{\partial[H^+]} = 1$$

Table D2. Coefficients for the partitioning of $\frac{d[H^+]}{dt}$ into contributions by modeled kinetic processes.

$$\alpha_{\mathbf{R}_{ox}}\left.\frac{\partial[TA]}{\partial[H^+]}\right|_{c,n} = \beta_{\mathbf{R}_{ox}} = 1 - \left(\gamma\left.\frac{\partial[TA]}{\partial[\sum CO_2]}\right|_{h,n} + \left.\frac{\partial[TA]}{\partial[\sum NH_4^+]}\right|_{h,c}\right)$$

$$\alpha_{\mathbf{R}_{nit}}\left.\frac{\partial[TA]}{\partial[H^+]}\right|_{c,n} = \beta_{\mathbf{R}_{nit}} = -2 + \left.\frac{\partial[TA]}{\partial[\sum NH_4^+]}\right|_{h,c}$$

$$\alpha_{\mathbf{E}_{CO_2}}\left.\frac{\partial[TA]}{\partial[H^+]}\right|_{c,n} = \beta_{\mathbf{E}_{CO_2}} = -\left.\frac{\partial[TA]}{\partial[\sum CO_2]}\right|_{h,n}$$

$$\alpha_{\mathbf{E}_{NH_3}}\left.\frac{\partial[TA]}{\partial[H^+]}\right|_{c,n} = \beta_{\mathbf{E}_{NH_3}} = 1 - \left.\frac{\partial[TA]}{\partial[\sum NH_4^+]}\right|_{h,c}$$

$$\sum \mathbf{T}\left.\frac{\partial[TA]}{\partial[H^+]}\right|_{c,n} = +\left(\mathbf{T}_{HCO_3^-} + 2\,\mathbf{T}_{CO_3^{2-}} + \mathbf{T}_{NH_3} - \mathbf{T}_{H^+}\right) - \left(\mathbf{T}_{CO_2} + \mathbf{T}_{HCO_3^-} + \mathbf{T}_{CO_3^{2-}}\right)\left.\frac{\partial[TA]}{\partial[\sum CO_2]}\right|_{h,n} - \left(\mathbf{T}_{NH_3} + \mathbf{T}_{NH_4^+}\right)\left.\frac{\partial[TA]}{\partial[\sum NH_4^+]}\right|_{h,c}$$

Acknowledgements. We thank D. Wolf-Gladrow for sharing his knowledge and expertise on seawater carbonate chemistry and pH modeling at various occasions. We thank B. P. Boudreau and an anonymous reviewer for their constructive criticism on an earlier version of this manuscript. This research was supported by the EU (Carbo-Ocean, 511176-2) and the Netherlands Organisation for Scientific Research (833.02.2002). This is publication 4230 of the Netherlands Institute of Ecology (NIOO-KNAW).

Edited by: Y. Prairie

References

Alley, R., Berntsen, T., Bindoff, N. L., et al.: Climate Change 2007: The Physical Science Basis – Summary for Policymakers (WGI contribution). Tech. Rep., Geneva, 2007.

Andersson, M. G. I., Brion, N., and Middelburg, J. J.: Comparison of nitrifier activity versus growth in the Scheldt estuary – a turbid, tidal estuary in northern Europe, Aquat. Microb. Ecol., 42(2), 149–158, 2006.

Aris, R. and Mah, R. H. S.: Independence of Chemical Reactions, Ind. Eng. Chem. Fund., 2(2), 90–94, 1963.

Ben-Yaakov, S.: A Method for Calculating the in Situ pH of Seawater, Limnol. Oceanogr., 15(2), 326–328, 1970.

Bjerknes, V. and Tjomsland, T.: Flow and pH modeling to study the effects of liming in regulated, acid salmon rivers, Water Air Soil Pollut., 130(1–4), 1409–1414, 2001.

Borges, A. V., Vanderborght, J. P., Schiettecatte, L. S., Gazeau, F., Ferron-Smith, S., Delille, B., and Frankignoulle, M.: Variability of the gas transfer velocity of CO_2 in a macrotidal estuary (the Scheldt), Estuaries, 27(4), 593–603, 2004.

Boudreau, B. P.: A Steady-State Diagenetic Model for Dissolved Carbonate Species and pH in the Porewaters of Oxic and Suboxic Sediments, Geochimica Et Cosmochimica Acta, 51(7), 1985–1996, 1987.

Boudreau, B. P.: Modelling the sulfide-oxygen reaction and associated pH gradients in porewaters, Geochimica et Cosmochimica Acta, 55(1), 145–159, 1991.

Boudreau, B. P.: A method-of-lines code for carbon and nutrient diagenesis in aquatic sediments, Computers Geosciences, 22(5), 479–496, 1996a.

Boudreau, B. P.: Diagenetic Models and Their Implementation, Springer, 1996b.

Boudreau, B. P. and Canfield, D. E.: A Provisional Diagenetic Model for Ph in Anoxic Porewaters - Application to the Foam Site, J. Mar. Res., 46(2), 429–455, 1988.

Boudreau, B. P. and Canfield, D. E.: A Comparison of Closed-System and Open-System Models for Porewater Ph and Calcite-Saturation State, Geochimica Et Cosmochimica Acta, 57(2), 317–334, 1993.

Bronstein, I., Semendjajew, K., Musiol, G., and Muehlig, H.: Taschenbuch der Mathematik, 4th Ed., Verlag Harri Deutsch, 1999.

Chilakapati, A., Ginn, T., Szecsody, J.: An analysis of complex reaction networks in groundwater modeling, Water Resour. Res., 34(7), 1767–1780, 1998.

Culberson, C. H.: Calculation of the In-situ pH of Seawater, Limnol. Oceanogr., 25(1), 150–152, 1980.

Dickson, A. G.: An Exact Definition of Total Alkalinity and a Procedure for the Estimation of Alkalinity and Total Inorganic Carbon from Titration Data, Deep-Sea Res. A, 28(6), 609–623, 1981.

Dickson, A. G.: pH Scales and Proton-Transfer Reactions in Saline Media Such as Sea-Water, Geochimica Et Cosmochimica Acta, 48(11), 2299–2308, 1984.

DiToro, D. M.: Combining Chemical Equilibrium and Phytoplankton Models – A General Methodology, in Modelling Biochemical Processes on Aquatic Ecosystems, edited by: Canale, R. P., Ann Arbor Science, 233–255, 1976.

DOE: Handbook of Methods for the Analysis of the Various Parameters of the Carbon Dioxide System in Sea Water, ORNL/CDIAC-74, 1994.

Fabian, G., Van Beek, D. A., and Rooda, J. E.: Index Reduction and Discontinuity Handling Using Substitute Equations, Math. Comp. Model. Dyn., 7(2), 173–187, 2001.

Follows, M. J., Ito, T., and Dutkiewicz, S.: On the solution of the carbonate chemistry system in ocean biogeochemistry models, Ocean Model., 12(3–4), 290–301, 2006.

Follows, M. J., Williams, R. G., and Marshall, J. C.: The solubility pump of carbon in the subtropical gyre of the North Atlantic, J. Mar. Res., 54(4), 605–630, 1996.

Frankignoulle, M.: A Complete Set of Buffer Factors for Acid-Base CO_2 System in Seawater, J. Mar. Syst., 5(2), 111–118, 1994.

Garcia, H. E. and Gordon, L. I.: Oxygen Solubility in Seawater – Better Fitting Equations, Limnol. Oceanogr., 37(6), 1307–1312, 1992.

Gehlen, M., Mucci, A., and Boudreau, B.: Modelling the distribution of stable carbon isotopes in porewaters of deep-sea sediments, Geochimica Et Cosmochimica Acta, 63(18), 2763–2773, 1999.

Heip, C.: Biota and Abiotic Environment in the Westerschelde Estuary, Hydrobiological Bulletin, 22(1), 31–34, 1988.

Hellings, L., Dehairs, F., Van Damme, S., and Baeyens, W.: Dissolved inorganic carbon in a highly polluted estuary (the Scheldt), Limnol. Oceanogr., 46(6), 1406–1414, 2001.

Jourabchi, P., Van Cappellen, P., and Regnier, P.: Quantitative interpretation of pH distributions in aquatic sediments: A reaction-transport modeling approach, Am. J. Sci., 305(9), 919–956, 2005.

Lichtner, P. C.: Continuum formulation of multicomponent-multiphase reactive transport, Reactive Transport in Porous Media, 34, 1–81, 1996.

Luff, R., Haeckel, M., and Wallmann, K.: Robust and fast FORTRAN and MATLAB (R) libraries to calculate pH distributions in marine systems, Computers Geosciences, 27(2), 157–169, 2001.

Marinelli, R. L. and Boudreau, B. P.: An experimental and modeling study of pH and related solutes in an irrigated anoxic coastal sediment, J. Mar. Res., 54(5), 939–966, 1996.

Meysman, F.: Modelling the influence of ecological interactions on reactive transport processes in sediments, Ph.D. thesis, Netherlands Institute of Ecology, University of Gent, 2001.

Meysman, F. J. R., Middelburg, J. J., Herman, P. M. J., and Heip, C. H. R.: Reactive transport in surface sediments. II. Media: an object-oriented problem-solving environment for early diagenesis, Computers Geosciences, 29(3), 301–318, 2003.

Middelburg, J. J., Klaver, G., Nieuwenhuize, J., Wielemaker, A.,

deHaas, W., Vlug, T., and van der Nat, J. F. W. A.: Organic matter mineralization in intertidal sediments along an estuarine gradient, Mar. Ecol.-Progress Ser., 132(1–3), 157–168, 1996.

Millero, F. J.: Thermodynamics of the Carbon-Dioxide System in the Oceans, Geochimica Et Cosmochimica Acta, 59(4), 661–677, 1995.

Moatar, F., Fessant, F., Poirel, A.: pH modeling by neural networks. Application of control and validation data series in the Middle Loire river, Ecol. Modell., 120(2–3), 141–156, 1999.

Morel, F. M. and Hering, J. G.: Principles and Applications of Aquatic Chemistry, John Wiley & Sons, 1993.

Olander, D. R.: Simultaneous Mass Transfer and Equilibrium Chemical Reaction, Aiche J., 6(2), 233–239, 1960.

Orr, J. C., Fabry, V. J., Aumont, O., Bopp, L., Doney, S. C., Feely, R. A., Gnanadesikan, A., Gruber, N., Ishida, A., Joos, F., Key, R. M., Lindsay, K., Maier-Reimer, E., Matear, R., Monfray, P., Mouchet, A., Najjar, R. G., Plattner, G. K., Rodgers, K. B., Sabine, C. L., Sarmiento, J. L., Schlitzer, R., Slater, R. D., Totterdell, I. J., Weirig, M. F., Yamanaka, Y., and Yool, A.: Anthropogenic ocean acidification over the twenty-first century and its impact on calcifying organisms, Nature, 437(7059), 681–686, 2005.

Otto, N. C. and Quinn, J. A.: Facilitated Transport of Carbon Dioxide through Bicarbonate Solutions, Chem. Eng. Sci., 26(6), 949–961, 1971.

Petzold, L. R.: A Description of DASSL: A Differential/Algebraic System Solver, in: IMACS World Congress, Sandia National Laboratories, Montreal, Canada, 1982.

Prentice, C., Farquhar, G. D., Fasham, M. J. R., Goulden, M. L., Heimann, M., and Jaramillo, V. J.: The carbon cycle and atmospheric carbon dioxide, in: Climate Change 2001: The Scientific Basis, edited by: Houghton, J., Ding, Y., Griggs, D. J., Noguer, M., van der Linden, P. J., and Xiaosu, D., Cambridge University Press, New York, 185–237, 2001.

Press, W., Teukolsky, S., and Vetterling, W.: Numerical recipes in FORTRAN: the art of scientific computing, 2nd Ed., Cambridge University Press, Cambridge, 1992.

Raymond, P. A. and Cole, J. J.: Gas exchange in rivers and estuaries: Choosing a gas transfer velocity, Estuaries, 24(2), 312–317, 2001.

Regnier, P., Wollast, R., and Steefel, C. I.: Long-term fluxes of reactive species in macrotidal estuaries: Estimates from a fully transient, multicomponent reaction-transport model, Mar. Chem., 58(1–2), 127–145, 1997.

Roy, R. N., Roy, L. N., Lawson, M., Vogel, K. M., Moore, C. P., Davis, W., and Millero, F. J.: Thermodynamics of the Dissociation of Boric-Acid in Seawater at S=35 from 0-Degrees-C to 55-Degrees-C, Mar. Chem., 44(2–4), 243–248, 1993.

Saaltink, M. W., Ayora, C., Carrera, J.: A mathematical formulation for reactive transport that eliminates mineral concentrations, Water Resour. Res., 34(7), 1649–1656, 1998.

Sarmiento, J. L. and Gruber, N.: Ocean Biogeochemical Dynamics, Princeton University Press, Princeton, 2006.

Soetaert, K., deClippele, V., and Herman, P.: FEMME, a flexible environment for mathematically modeling the environment, Ecol. Modell., 151(2–3), 177–193, 2002.

Soetaert, K. and Herman, P.: MOSES Model of the Schelde Estuary – Ecosystem Development under SENECA, Tech. Rep., Netherlands Institute of Ecology, 1994.

Soetaert, K. and Herman, P. M. J.: Carbon Flows in the Westerschelde Estuary (the Netherlands) Evaluated by Means of an Ecosystem Model (Moses), Hydrobiologia, 311(1–3), 247–266, 1995a.

Soetaert, K. and Herman, P. M. J.: Nitrogen Dynamics in the Westerschelde Estuary (Sw Netherlands) Estimated by Means of the Ecosystem Model Moses, Hydrobiologia, 311(1–3), 225–246, 1995b.

Soetaert, K., Hofmann, A. F., Middelburg, J. J., Meysman, F. J., and Greenwood, J.: The effect of biogeochemical processes on pH, Mar. Chem., 105(1–2), 30–51, 2007.

Soetaert, K., Middelburg, J. J., Heip, C., Meire, P., Van Damme, S., and Maris, T.: Long-term change in dissolved inorganic nutrients in the heterotropic Scheldt estuary (Belgium, The Netherlands), Limnol. Oceanogr., 51(1, part 2), 409–423, 2006.

Steefel, C. I. and MacQuarrie, K. T. B.: Approaches to modeling of reactive transport in porous media, Reactive Transport in Porous Media, 34, 83–129, 1996.

Stumm, W. and Morgan, J. J.: Aquatic Chemistry: Chemical Equilibria and Rates in natural Waters, Wiley Interscience, New York, 1996.

Thomann, R. V. and Mueller, J. A.: Principles of Surface Water Quality Modeling and Control, Harper & Row, New York, 1987.

Wang, Y. F. and Van Cappellen, P.: A multicomponent reactive transport model of early diagenesis: Application to redox cycling in coastal marine sediments, Geochimica Et Cosmochimica Acta, 60(16), 2993–3014, 1996.

Wanninkhof, R.: Relationship between Wind-Speed and Gas-Exchange over the Ocean, J. Geophys. Res.-Oceans, 97(C5), 7373–738, 19922.

Weiss, R. F.: Carbon dioxide in water and seawater: the solubility of a non-ideal gas, Mar. Chem., 2, 203–215, 1974.

Wolf-Gladrow, D. A., Zeebe, R. E., Klaas, C., Koertzinger, A., Dickson, A. G.: Total alkalinity: the explicit conservative expression and its application to biogeochemical processes, Mar. Chem., 106(1–2), 287–300, 2007.

Zeebe, R. E.: Modeling CO_2 chemistry, δ13C, and oxidation of organic carbon and methane in sediment porewater: Implications for paleo-proxies in benthic foraminifera, Geochimica et Cosmochimica Acta, 71(13), 3238–325, 2007.

Zeebe, R. E. and Wolf-Gladrow, D.: CO_2 in Seawater: Equilibrium, Kinetics, Isotopes, 1st Ed., No. 65, Elsevier Oceanography Series, Elsevier, 2001.